

# Chapter 4

## Electrical Conductivity of Carbon Nanotube- and Graphene-Based Nanocomposites

Yang Wang and George J. Weng

**Abstract** Carbon nanotube- and graphene-based polymer nanocomposites are known to have exceptional electrical conductivity even at very low filler loading. In this chapter we present a widely useful composite model for studying this property. This model has the capability of determining both the effective electrical conductivity and the percolation threshold of the nanocomposites. It also embodies several other important elements of the process of conduction, including filler loading, filler agglomeration, anisotropic property of carbon fillers, effect of imperfect interfaces, and the contribution of electron tunneling. The backbone of the model is the effective-medium theory with a perfect interface; it can demonstrate the percolation feature and can also comply with the Hashin-Shtrikman bounds. To study the influence of filler agglomeration, a two-scale approach is further proposed. The imperfect interface is incorporated into the model by the introduction of a thin, weak interface surrounding each inclusion. To account for the effect of electron tunneling, Cauchy's statistical distribution function is further introduced to reflect the increased activity of electron tunneling at and after the percolation threshold. It is demonstrated that the theoretical predictions based on the developed model are in close agreement with available experimental data.

### 4.1 Introduction

With the growth of nanotechnology in recent years, a new kind of nanocomposites has emerged for their enhanced mechanical, thermal, and electrical performance. This class of nanocomposites generally consists of a polymer matrix and various types of carbon fillers, such as graphite, carbon nanofiber, carbon nanotube (CNT), and graphene. Two of the most attractive fillers are carbon nanotubes and graphene.

---

Y. Wang • G.J. Weng (✉)

Department of Mechanical and Aerospace Engineering, Rutgers University,  
New Brunswick, NJ 08903, USA

e-mail: [yang.wang@rutgers.edu](mailto:yang.wang@rutgers.edu); [gjweng@soe.rutgers.edu](mailto:gjweng@soe.rutgers.edu)

Both are known to possess very high mechanical stiffness and tensile strength, as well as exceptional thermal and electrical conductivity. For electrical conductivity, it can be as high as  $10^6$  to  $10^7$  S/m for pure CNT and  $10^8$  S/m for pure graphene. These values are comparable to the two best kinds of metal conductor, silver and copper, which have  $6.30 \times 10^7$  and  $5.96 \times 10^7$  S/m, respectively. This remarkable electrical conductivity is due to the microstructure of CNT and graphene. Graphene is an allotrope of carbon that comes in the form of a one-atom-thick two-dimensional layer of  $sp^2$ -bonded carbon atoms. All atoms are arranged in a honeycomb grid sheet, so that each one of them is bonded with another three (Allen et al. 2010). This two-dimensional single-layered graphene sheet is the basic structural element of other allotropes of carbon. It can be rolled up into a hollow cylindrical structure to get the one-dimensional CNT, while the honeycomb grid for carbon atoms remains unchanged (Geim and Novoselov 2007). Since each carbon atom has four electrons in the outer shell and only three are used to form covalent bonds, there is one remaining electron that is highly mobile and available for electrical conduction. As a consequence, both CNT and graphene are highly conductive. In experiments, their intrinsic electrical conductivities are usually reported on the orders of  $10^3$  to  $10^5$  S/m. In contrast the electrical conductivity of most polymers is measured on the orders of  $10^{-15}$  to  $10^{-8}$  S/m. This makes the property contrast between the inclusion and matrix phase on the orders of  $10^{12}$  to  $10^{18}$ . Therefore the electrical conductivity of CNT and graphene-based nanocomposites is a high-contrast problem, and it is significantly different from the classical problem of elastic property in fiber-reinforced composites where the material property contrast is only on the order of  $10^2$ .

Another great feature for CNT and graphene-based nanocomposites is the percolation phenomenon. As the loading of carbon fillers in the nanocomposites increases, the growth of overall electrical conductivity does not follow a linear rule of mixture. Around certain filler concentrations, its value can grow dramatically for several orders of magnitude, so that the whole composite turns from almost insulating to highly conductive. This rapid growth of overall electrical conductivity around a critical filler concentration is the percolation phenomenon, which usually occurs in composites whose constituent properties have very high contrast. It is also a transitional stage in which the overall property of the composite shifts from the property of matrix phase to that of the inclusion phase, and the onset of this transition is the percolation threshold. At microscopic scale the percolation phenomenon indicates that the conductive fillers are not surrounded by the insulating matrix anymore. Instead they have contact with each other; thus a conductive network is formed and expanded throughout the composite (Nan et al. 2010). The electric current can now flow into this conductive network, without having to bypass the barrier of insulating matrix. Therefore the overall electrical conductivity of the composite is tremendously improved. The value of percolation threshold is mainly governed by the geometrical structure of the composite. One important parameter that characterizes this geometrical structure is the aspect ratio (length-to-diameter ratio) of the inclusion. As mentioned above, graphene has a microstructure of flat sheet so that it can be treated as a spheroid with a very small (usually less than 0.01) aspect ratio, while the aspect ratio of CNT is very large (usually more than

100) due to its long cylinder microstructure. Because of these two kinds of extreme aspect ratios, the percolation thresholds for CNT and graphene fillers are generally very low. This means that we can achieve highly conductive nanocomposites with only a small amount of CNT or graphene loading, which is definitely a desirable characteristic. For example, Gardea and Lagoudas (2014) reported a remarkable 10-order of magnitude increase in the overall electrical conductivity at 0.1 wt.% of pristine CNTs for a CNT/epoxy nanocomposite. He and Tjong (2013) prepared a graphene/polyvinylidene fluoride nanocomposite with a percolation threshold of 0.31 graphene vol.%, while the graphene/polyethylene nanocomposite fabricated by Pang et al. (2010) had an even lower 0.07 vol.%. In short, with high property contrast and extreme aspect ratios, CNTs and graphene are the ideal reinforcements for nanocomposites that can substantially enhance the overall electrical conductivity at very low filler loading.

Because of these geometrical similarities, one can study CNT- and graphene-based nanocomposites together under the same theoretical framework, with only a slight difference being their very long cylinder and thin plate structure. The theoretical study of CNT and graphene-based nanocomposites involves two major issues: (1) the determination of the overall electrical conductivity and (2) the determination of percolation threshold. In retrospect, many investigations have been separately made upon these two issues. For the first one, a simple and widely used empirical model for calculating the effective electrical conductivity,  $\sigma_e$ , is the scaling law with the dependence on filler concentration  $c_1$ , as (e.g., Bauhofer and Kovacs 2009)

$$\sigma_e = \sigma_0 (c_1 - c_1^*)^t, \quad (4.1)$$

where  $c_1^*$  is the percolation threshold and  $\sigma_0$  and  $t$  are the two fitting parameters. This model offers an easy way of curve fitting with the experimental data, but it gives no insights into the physical mechanism of the conduction process. More advanced models that have been developed from the perspective of micromechanics are later brought into the study of electrical conductivity. They can incorporate the issues such as the volume concentration, shape, and orientations of carbon fillers. Among these models, the most widely used ones include the Mori–Tanaka (M–T) method (Mori and Tanaka 1973), the Ponte Castañeda–Willis (PCW) model (Castañeda and Willis 1995), and Bruggeman’s effective-medium approach (Bruggeman 1935). A comprehensive development of the M–T method was provided by Weng (1984) and Benveniste (1987) in the elastic context and by Hatta and Taya (1985) and Nan et al. (1997) for thermal conductivity. The PCW model was also originally developed for the elastic properties and was applied to thermal and electrical conductivity by Duan et al. (2006) and Pan et al. (2011), respectively. As the PCW model could easily go out of the Hashin–Shtrikman (H–S) upper bound (Hashin and Shtrikman 1962) beyond certain inclusion concentration, Pan et al. (2011) also suggested using the H–S upper bound to guide the development of electrical conductivity after PCW model hit the bound. The effective-medium approach is a symmetric version of the self-consistent method that is also called the coherent potential approximation. It has a realizable microstructure and treats both the inclusion and matrix on equal, symmetric footing. With spherical inclusions it was first applied by

Landauer (1952) to study the effective electrical conductivity of a metallic mixture with spherical particles. In the mechanical context, it was first developed by Hill (1965) and Budiansky (1965). It should be noted that many notable contributions to the study of electrical conductivity have been made in recent years under the framework of micromechanics. For instance, Xie et al. (2008) adopted another form of the self-consistent method, which relied solely on the average field concentration of the randomly oriented ellipsoids, to compare the electrical conductivity between composites reinforced by CNT and graphene nanosheets. Deng and Zheng (2008) provided an analytical model with the consideration of the percolation probability of CNT inclusions. Seidel and Lagoudas (2009) and Feng and Jiang (2013) both used the composite cylinder method to solve for the electric fields in a microscale representative volume element. All these works have provided significant insights for the physical principle of conduction process and the microstructure of the nanocomposites.

The determination of percolation threshold has also been extensively studied by both numerical methods and some analytical models. Due to the random orientation and distribution of carbon fillers, Monte Carlo (MC) simulations, such as the works by Li and Chou (2007) and Ma et al. (2010), have often been invoked to numerically investigate the percolation threshold. However MC simulation is computationally expensive. There are other theoretical approaches that focus on the geometry of percolation network. For instance, Balberg et al. (1984) considered 3-D randomly oriented sticks combined with their associated average excluded volume, Bao et al. (2013) randomly generated cylinder models in the representative volume and proposed a percolating network recognition scheme with periodic boundary conditions, and Chatterjee (2013) used a polydisperse system of rods with the help of Bethe lattice site percolation model. These models have the merit of providing analytical results for the percolation threshold, but they are under a totally different theoretical framework from the micromechanics theories. Some of the preceding continuum composite models have to borrow the percolation threshold from other numerical results; it implies that such composite models are not self-contained to be able to cover the overall electrical conductivity and percolation threshold simultaneously. This is an issue that we want to avoid here. In what follows, we will show that, in our continuum model, the percolation threshold is an integral part of the continuum theory can be directly derived.

There are some additional problems that affect the overall electrical conductivity and percolation threshold of CNT and graphene-based nanocomposites. We consider three important ones: (1) the filler agglomeration, (2) the imperfect interface effect, and (3) the effect of electron tunneling. The first problem is related to the inhomogeneous dispersion state of carbon fillers in the composite. In certain cases a lot of CNT or graphene fillers tend to cluster together to form many filler agglomerations. Inside each agglomerate, carbon fillers are highly dense, more so than the rest of the composite. This phenomenon can be observed from various TEM images of CNT and graphene-based nanocomposites. It is mainly caused by the different processing routes of CNT and graphene samples. For instance, graphene can be produced by the liquid-phase exfoliation of graphite, or by the thermal reduction of graphite oxide. The former gives more dispersed graphene samples

while the latter results in more graphene agglomerations. Filler agglomerations change the microstructure of the nanocomposites, so it is necessary to investigate its effect on the overall electrical conductivity and percolation threshold. A few experimental results—including those by Martin et al. (2004), Hernández et al. (2009), Aguilar et al. (2010)—have suggested that CNT agglomerations could favor the formation of CNT conductive network and improve the effective electrical conductivity. A theoretical study by Li et al. (2007a, b) has treated CNT agglomerations to be of spherical shape and calculated the percolation threshold based on the corresponding inter-particle distance. However it was not capable of predicting the overall electrical conductivity, so a thorough theoretical analysis of the effect of filler agglomeration was not completed. To this end, we will adopt a two-scale approach as suggested by Barai and Weng (2011) in the study of CNT-based metal plasticity to address the issue of filler agglomeration.

The second problem—the imperfect interface effect—has a long history in the study of composite materials. In general the bonding between the inclusion and matrix is not ideally perfect, and there exists a weak interface that could diminish the overall property of the composite. In the context of thermal conductivity, Dunn and Taya (1993), Duan and Karihaloo (2007), and Nan et al. (1997) have extended the micromechanics formulation to account for the imperfect interface condition. Hashin (2001) also proposed a generalized theory for the imperfect interface of conduction, dielectric behavior, and permeability. A common theoretical treatment for an imperfect interface is to model it as a thin interphase between two constituent phases. Compared with the original inclusion, the interphase has lower electrical conductivity, or in terms of its counterpart, higher electrical resistivity. With a diminishing thickness, the interphase becomes a layer of interface surrounding the original inclusion, so that it turns into a thinly coated inclusion. The overall electrical conductivity of this coated inclusion is lowered due to the interfacial resistance of the interface layer, and this signifies the effect of imperfect interfaces. The last problem on the effect of electron tunneling has received less attention from the continuum perspective. But it has been numerically studied by MC simulations, such as the works by Bao et al. (2012) and Li et al. (2007a, b). MC simulations are highly computational, while our objective is to develop a continuum scheme that could have both simplicity and wide applicability. Electron tunneling is a quantum mechanical effect that electrons can jump from one carbon filler to another adjacent one, over the barrier of an insulating polymer matrix. It gives rise to the tunneling-assisted interfacial conductivity which could enhance the overall electrical conductivity of the nanocomposite. This contribution is incorporated into our model by reducing the interfacial resistance. Finally, considering the probabilistic nature of electron hopping, the reduction of interfacial resistance is further characterized by Cauchy's statistical distribution function. In this way, the effects of imperfect interfaces and electron tunneling can all be taken into account.

In the following we will first introduce the effective-medium theory to determine the overall electrical conductivity of a nanocomposite with a perfect interface. This will be followed with the derivation of percolation threshold. Then the effects of filler agglomeration, imperfect interface, and electron tunneling will be

subsequently added into the model. To verify the applicability of the developed model, three sets of experimental data on CNT and graphene-based nanocomposites will be analyzed and compared with the calculated results.

## 4.2 The Theory

### 4.2.1 *Effective-Medium Theory with a Perfect Interface*

The microstructure of CNT and graphene-based nanocomposites can be conceived to be a two-phase composite, with carbon fillers as the inclusions and polymer binder as the matrix. All inclusions are assumed to have spheroidal shapes. CNT inclusions correspond to prolate spheroids with high aspect ratios. Compared with long cylindrical CNTs, a prolate spheroidal CNT will possess almost the same shape when its aspect ratio is sufficiently large. Similarly, graphene inclusions are represented by oblate spheroids with very low aspect ratios, and they can recover the flat sheet graphene model when their aspect ratios are close to zero. The dispersion state of CNT and graphene inclusions is considered to be homogeneous and their orientations are totally random. This microstructure is schematically shown in Fig. 4.1. As the volume concentration of carbon inclusions increases, it becomes possible for them to have contact with each other. Those inclusions in touch can form a percolating path as shown by the red dashed line in Fig. 4.1. All percolating paths together become a conductive network, so that the electrical current can flow in this network without having to bypass the insulating matrix. The formation of the conductive network is exactly the percolation phenomenon at the microscopic scale.

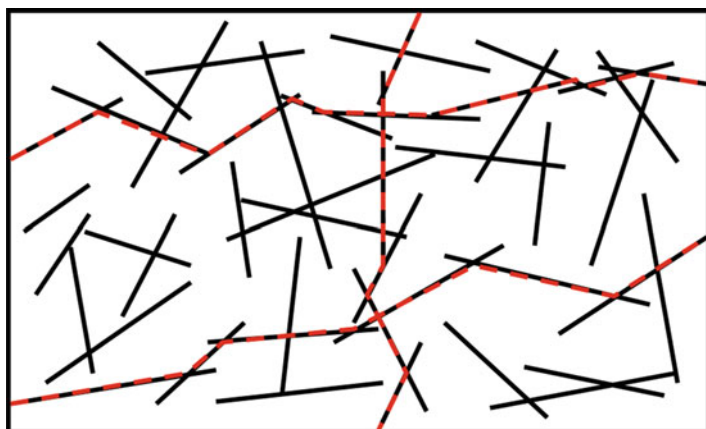


**Fig. 4.1** The microstructure of CNT and graphene-based nanocomposites, showing carbon fillers (*black solid line*) in the effective medium and three percolating paths (one vertical and two horizontal, in *red dashed line*)

To study this phenomenon by micromechanics, we now introduce the effective-medium theory. There are several ways to derive this theory. One of the most attractive ways is to adopt Maxwell’s far-field matching (Maxwell 1891) of the scattered fields between the two-phase composite and the homogenized effective medium (Weng 2010). If we denote the moduli tensor of the reference medium in which the scattered fields of the two-phase composite and the homogeneous effective medium are to be evaluated by  $\mathbf{L}_r$ , the moduli tensor of the effective medium by  $\mathbf{L}_e$ , and those of the matrix and inclusion phase by  $\mathbf{L}_0$  and  $\mathbf{L}_1$ , respectively, then the scattered tensor  $\mathbf{T}_i$  of phase  $i$  can be written as

$$\mathbf{T}_i = \left[ (\mathbf{L}_i - \mathbf{L}_r)^{-1} + \mathbf{S}_i \mathbf{L}_r^{-1} \right]^{-1}, \tag{4.2}$$

where  $\mathbf{S}_i$  is the Eshelby S-tensor (Eshelby 1957) of  $i$ th phase in the reference medium. Now denote the volume concentrations of the matrix and inclusion phase by  $c_0$  and  $c_1$ , respectively, then Maxwell’s far-field matching requires that the scattered fields from the effective medium and the sum of scattered fields from two individual phases are equal, which leads to  $\mathbf{T}_e = c_0 \mathbf{T}_0 + c_1 \mathbf{T}_1$ , or

$$\begin{aligned} \left[ (\mathbf{L}_e - \mathbf{L}_r)^{-1} + \mathbf{S}_e \mathbf{L}_r^{-1} \right]^{-1} &= c_0 \left[ (\mathbf{L}_0 - \mathbf{L}_r)^{-1} + \mathbf{S}_0 \mathbf{L}_r^{-1} \right]^{-1} \\ &+ c_1 \left[ (\mathbf{L}_1 - \mathbf{L}_r)^{-1} + \mathbf{S}_1 \mathbf{L}_r^{-1} \right]^{-1}. \end{aligned} \tag{4.3}$$

In the effective-medium approach, the property of the reference medium  $\mathbf{L}_r$  is chosen to be equal to that of the effective medium,  $\mathbf{L}_e$ , so that the scattered field on the left of Eq. (4.3) automatically vanishes. This leads to the final equation for the effective-medium approach

$$c_0 \left[ (\mathbf{L}_0 - \mathbf{L}_e)^{-1} + \mathbf{S}_0 \mathbf{L}_e^{-1} \right]^{-1} + c_1 \left[ (\mathbf{L}_1 - \mathbf{L}_e)^{-1} + \mathbf{S}_1 \mathbf{L}_e^{-1} \right]^{-1} = \mathbf{0}. \tag{4.4}$$

The effective property of this two-phase composite can be obtained by solving Eq. (4.4) for tensor  $\mathbf{L}_e$  at any given inclusion volume concentration,  $c_1$ .

In CNT and graphene-based nanocomposites, the moduli tensor for the electrical conductivity,  $\mathbf{L}$ , is a second-order tensor, which is defined by

$$J_i = L_{ij} E_j, \tag{4.5}$$

where vector  $\mathbf{J}$  and  $\mathbf{E}$  are the electric current density and electric field. In addition, due to the microstructure of CNT and graphene, their properties are transversely isotropic, with 3-direction as the symmetric direction, and plane 1–2 as the isotropic plane (they also coincide with the symmetric direction and isotropic plane of the spheroidal model of CNT and graphene inclusion). For the polymer matrix, it has no particular orientation in the microstructure; thus its property is isotropic. As a

result, the moduli tensors for the polymer matrix,  $\mathbf{L}_0$ , and carbon inclusions,  $\mathbf{L}_1$ , can be expressed as

$$\mathbf{L}_0 = \begin{bmatrix} \sigma_0 & 0 & 0 \\ 0 & \sigma_0 & 0 \\ 0 & 0 & \sigma_0 \end{bmatrix}, \quad \text{and} \quad \mathbf{L}_1 = \begin{bmatrix} \sigma_1 & 0 & 0 \\ 0 & \sigma_1 & 0 \\ 0 & 0 & \sigma_3 \end{bmatrix}, \quad (4.6)$$

where  $\sigma_0$  is the electrical conductivity of the polymer matrix, and  $\sigma_1$  and  $\sigma_3$  are that of carbon inclusions along the in-plane and normal directions. In general, it is much more conductive along the CNT length and in the graphene plane; thus we have  $\sigma_1 \ll \sigma_3$  for CNT inclusions and  $\sigma_1 \gg \sigma_3$  for graphene inclusions. It is convenient to introduce a constant  $m$  to describe this anisotropy relation as  $\sigma_1 = m\sigma_3$ , so that  $m < 1$  for CNT and  $m > 1$  for graphene. Still both  $\sigma_1$  and  $\sigma_3$  are much larger than  $\sigma_0$ , since the polymer is an electrically insulating material. Likewise, the Eshelby S-tensor for the two phases,  $\mathbf{S}_0$  and  $\mathbf{S}_1$ , are also isotropic and transversely isotropic, respectively, such that

$$\mathbf{S}_0 = \begin{bmatrix} S_{00} & 0 & 0 \\ 0 & S_{00} & 0 \\ 0 & 0 & S_{00} \end{bmatrix}, \quad \text{and} \quad \mathbf{S}_1 = \begin{bmatrix} S_{11} & 0 & 0 \\ 0 & S_{11} & 0 \\ 0 & 0 & S_{33} \end{bmatrix}. \quad (4.7)$$

With 3-direction as the symmetric axis of the spheroidal inclusion, the components of  $\mathbf{S}_1$  depend on the inclusion aspect ratio,  $\alpha$ , as

$$S_{11} = S_{22} = \begin{cases} \frac{\alpha}{2(1-\alpha^2)^{\frac{3}{2}}} \left[ \cos^{-1}\alpha - \alpha(1-\alpha^2)^{\frac{1}{2}} \right], & \alpha < 1 \\ \frac{\alpha}{2(\alpha^2-1)^{\frac{3}{2}}} \left[ \alpha(\alpha^2-1)^{\frac{1}{2}} - \cosh^{-1}\alpha \right], & \alpha > 1 \end{cases} \quad (4.8)$$

and  $S_{33} = 1 - 2S_{11}$  (the sum of all three diagonal components of S-tensor is 1). For the prolate-shaped CNT, its aspect ratio is always larger than 1, and  $0 < \alpha < 1$  corresponds to the oblate shape of graphene. When  $\alpha \rightarrow \infty$  (long fiber), these components are reduced to  $S_{11} = S_{22} = 1/2$  and  $S_{33} = 0$ , and when  $\alpha \rightarrow 0$  (thin plate), they are reduced to  $S_{11} = S_{22} = 0$  and  $S_{33} = 1$ . For spherical inclusions,  $\alpha = 1$  and each S-tensor component is  $1/3$ . On the other hand, since  $\mathbf{S}_0$  is isotropic, it should carry the same diagonal components in all three directions so that  $S_{00} = 1/3$ . Since the orientations of CNT and graphene inclusions are totally random, the overall nanocomposites must demonstrate isotropic property, and thus  $\mathbf{L}_e$  carries the same component  $\sigma_e$  in all three directions. At the same time we should also implement the effective-medium approach with its 3-D random version. Denoting the orientational average of a tensor by angular brackets,  $\langle \cdot \rangle$ , the equation for the 3-D random effective-medium approach can be written as

$$c_0 \left\langle \left[ (\mathbf{L}_0 - \mathbf{L}_e)^{-1} + \mathbf{S}_0 \mathbf{L}_e^{-1} \right]^{-1} \right\rangle + c_1 \left\langle \left[ (\mathbf{L}_1 - \mathbf{L}_e)^{-1} + \mathbf{S}_1 \mathbf{L}_e^{-1} \right]^{-1} \right\rangle = \mathbf{0}. \quad (4.9)$$



For any second-order tensor, its orientational average is given by the mean of three diagonal components times the second-order identity tensor,  $\delta_{ij}$ . Therefore Eq. (4.9) can be simplified from a tensor equation to a scalar equation as

$$c_0 \frac{\sigma_0 - \sigma_e}{\sigma_e + (1/3)(\sigma_0 - \sigma_e)} + c_1 \frac{1}{3} \left[ \frac{2(\sigma_1 - \sigma_e)}{\sigma_e + S_{11}(\sigma_1 - \sigma_e)} + \frac{\sigma_3 - \sigma_e}{\sigma_e + S_{33}(\sigma_3 - \sigma_e)} \right] = 0. \quad (4.10)$$

Solving this implicit equation for  $\sigma_e$ , the effective electrical conductivity of CNT and graphene-based nanocomposites is then obtained. To explain why the effective-medium approach is selected as the backbone of our model, we make a comparison among the effective-medium approach, the M-T method, and the PCW model. Besides, it is helpful to examine these three models in light of the H-S upper and lower bounds. Because these two bounds have been widely used as the maximum and minimum limit for the effective properties of composite materials, any valid estimation of effective properties should stay within the range of them. For simplicity, we make a preliminary study of the effective electrical conductivity of a two-phase composite with isotropic CNT inclusions and polymer matrix (phase 0 for the polymer matrix and phase 1 for the spheroidal CNT inclusion). In this setting, the M-T and PCW results for the effective electrical conductivity can be explicitly written as

$$\frac{\sigma_e^{\text{MT}}}{\sigma_0} = 1 + \frac{c_1 T}{1 - c_1 [1 - T/(n-1)]} \quad \text{and} \quad \frac{\sigma_e^{\text{PCW}}}{\sigma_0} = 1 + \frac{c_1 T}{1 - c_1 T/3}, \quad (4.11)$$

where

$$T = \frac{n-1}{3} \left[ \frac{2}{1 + (n-1)S_{11}} + \frac{1}{1 + (n-1)S_{33}} \right]. \quad (4.12)$$

It is noted that  $S_{11}$  and  $S_{33}$  are defined in Eq. (4.8), and  $n = \sigma_1/\sigma_0$  is the normalized electrical conductivity of the CNT inclusion. The results for the H-S upper and lower bounds (denoted by “+” and “-” sign) are given by

$$\begin{aligned} \frac{\sigma_e^{\text{HS}(+)}}{\sigma_0} &= 1 + \frac{(1-c_1)(1-n)}{(1/3)c_1(1-n) + n} \quad \text{and} \\ \frac{\sigma_e^{\text{HS}(-)}}{\sigma_0} &= 1 + \frac{c_1(n-1)}{(1/3)(1-c_1)(n-1) + 1}. \end{aligned} \quad (4.13)$$

Taking  $n = 10^{10}$  and the aspect ratio  $\alpha = 20$  as the properties of CNT inclusions, we calculate the results of effective electrical conductivity given by these three models and the two H-S bounds and plot them in logarithmic scale in Fig. 4.2. It is seen that the PCW result quickly goes out of the H-S upper bound at a CNT volume concentration of  $c_1 < 0.1$ . In strict applications, this theory is limited to the range

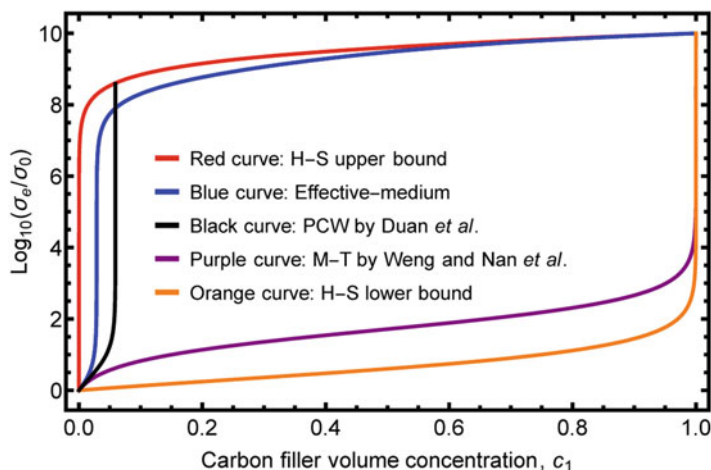


**Fig. 4.2** The examination of the effective-medium approach, the Mori-Tanaka method (Mori and Tanaka 1973) by Weng (1984, 1990) and Nan et al. (1997), and the Ponte Castañeda-Willis method (Castañeda and Willis 1995) by Duan et al. (2006) in light of the Hashin and Shtrikman (1962) bounds

$c_1 < 1/\alpha^2$ , which is 0.0025 here, but it can go a bit higher before it hits the H-S upper bound. This shows that the PCW model cannot properly yield the effective electrical conductivity over the entire range of  $c_1$ . In fact it was originally developed in a mechanical setting where the elastic properties of the inclusion and matrix phase have very little contrast (usually less than 10 times). But the electrical conductivity is an extremely high-contrast problem, which would cause the PCW result to have singularity at certain value of  $c_1$ . Therefore the PCW model is not suitable to account for a high-contrast, high aspect ratio problem. Both the effective-medium and the M-T results are seen to stay within the bounds, but the M-T result has no early percolation feature. Its curve stays rather flat at low CNT concentration and only when  $c_1$  approaches 1 does it start to grow rapidly, which is close to the trend of the H-S lower bound. Only the effective-medium result displays a sharp increase at low CNT concentration and possesses a percolation threshold, which is very close to the H-S upper bound at low volume concentration but is still always lower than it. In the microstructure of CNT or graphene nanocomposites, since a large amount of nanofillers are in contact with each other to form a conductive network, the CNT or graphene inclusions cannot be considered to be directly “embedded” in the polymer matrix any more. They are somewhat embedded in the effective medium, and therefore the effective-medium approach is a very appropriate model to study the effective electrical conductivity.

### 4.2.2 The Percolation Threshold

The percolation threshold of the nanocomposite,  $c_1^*$ , can be directly derived from Eq. (4.10) (Wang et al. 2014). This is done with the observation that, when the matrix phase is totally insulating ( $\sigma_0 = 0$ ), the effective electrical conductivity  $\sigma_e$  is entirely controlled by the conductive network of CNT and graphene inclusions, so the inclusion volume concentration  $c_1$  that first gives rise to a non-negative value of  $\sigma_e$  represents the percolation threshold,  $c_1^*$ . With  $\sigma_0 = 0$ , Eq. (4.10) turns into a quadratic equation for  $\sigma_e$ , in the following form

$$A\sigma_e^2 + B\sigma_e + C = 0, \quad (4.14)$$

with coefficient A, B, and C all being functions of  $c_1$ , as

$$\begin{aligned} A &= 9(1 - S_{33}^2) + c_1(1 - 3S_{33})^2, \\ B &= \sigma_1 \left[ -3c_1(1 - S_{33})(5 - 3S_{33}) + 9(1 - S_{33})^2 \right] + \sigma_3 \left[ -c_1(9S_{33}^2 + 3S_{33} + 2) \right. \\ &\quad \left. + 9S_{33}(1 + S_{33}) \right], \\ C &= \sigma_1\sigma_3 \left[ -c_1(-9S_{33}^2 + 15S_{33} + 2) + 9S_{33}(1 - S_{33}) \right], \end{aligned} \quad (4.15)$$

where the relation  $2S_{11} + S_{33} = 1$  has been used. As  $c_1$  increases from zero, initially all three coefficients are positive, so there is no positive solution for  $\sigma_e$  at very low  $c_1$ . When  $c_1$  reaches a critical value, there is a solution  $\sigma_e = 0$ , and as  $c_1$  further increases there is a positive solution for  $\sigma_e$ . This is the generally sought effective electrical conductivity with a perfectly insulating matrix, whereas the critical value of  $c_1$  giving rise to  $\sigma_e = 0$  is exactly the percolation threshold,  $c_1^*$ . This occurs when the coefficient  $C = 0$ , and this relation provides the value

$$c_1^* = \frac{9S_{33}(1 - S_{33})}{-9S_{33}^2 + 15S_{33} + 2}. \quad (4.16)$$

Since the S-tensor component  $S_{33}$  only depends on inclusion aspect ratio,  $\alpha$ , the percolation threshold is thus a strictly geometrical parameter. To see its effects, we plot its dependence on  $\alpha$  in Fig. 4.3, as  $\alpha$  increases from almost 0 (graphene-like) to infinity (CNT-like). For CNT- and graphene-based nanocomposites, the percolation thresholds with extreme values of  $\alpha$  are further illustrated in the insets. One can see that CNT provides a lower percolation threshold than the graphene with reciprocal aspect ratio. This is consistent with the result predicted by Pan et al. (2011). It can be also seen that the maximum value that  $c_1^*$  can attain is exactly 1/3, which corresponds to spherical inclusions, with  $\alpha = 1$ . This value has been widely reported in the literature.

The percolation threshold  $c_1^*$  can also be derived from Eq. (4.10) following a procedure suggested by Gao and Li (2003). In general, the matrix is almost insulating while inclusions are highly conductive. Therefore  $\sigma_i$  ( $i = 1$  or  $3$ , the

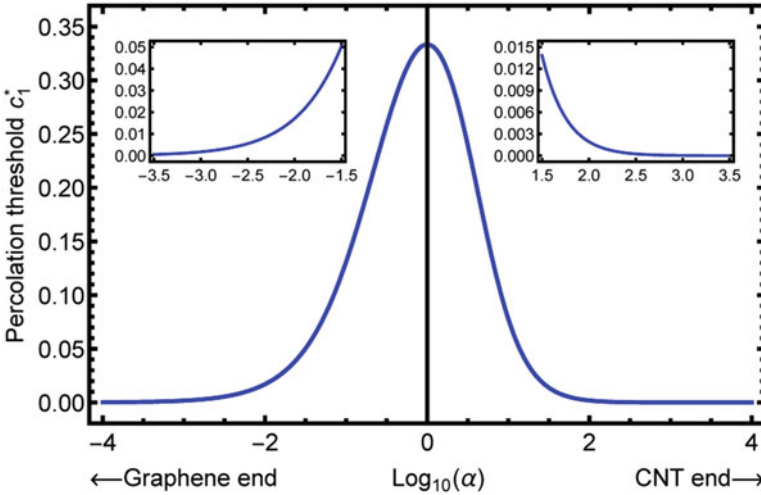


**Fig. 4.3** The dependence of percolation threshold on inclusion aspect ratio. The left-hand side is the graphene side while the right-hand side is the CNT side

same below) are usually several orders of magnitude higher than  $\sigma_0$ , which makes  $\sigma_0/\sigma_i \rightarrow 0$ . According to the percolation theory, when inclusion concentration  $c_1 < c_1^*$ ,  $\sigma_e$  has almost the same order of magnitude as  $\sigma_0$ , therefore  $\sigma_e/\sigma_i \rightarrow 0$ ; but after  $c_1^*$ ,  $\sigma_e$  will quickly approach  $\sigma_i$ , making  $\sigma_e/\sigma_0 \rightarrow \infty$ . Therefore at  $c_1 = c_1^*$ ,  $\sigma_e$  is at the transition stage, satisfying both  $\sigma_e/\sigma_0 \rightarrow \infty$  and  $\sigma_e/\sigma_i \rightarrow 0$  at the same time. Applying these two conditions to Eq. (4.10) and solving for  $c_1^*$ , one finds

$$c_1^* = \frac{3/(1 - S_0)}{3/(1 - S_0) + 1/S_{11} + 1/S_{22} + 1/S_{33}} = \frac{9S_{33}(1 - S_{33})}{-9S_{33}^2 + 15S_{33} + 2}, \quad (4.17)$$

which is exactly the same result as Eq. (4.16).

### 4.2.3 The Two-Scale Composite Model for Filler Agglomeration

In previous sections, we have assumed CNT and graphene-based nanocomposites to be homogeneous. However, the inhomogeneous distribution of CNT and graphene fillers, or filler agglomeration, is inevitable in reality. A good way to study the effect of filler agglomeration is to adopt a two-scale approach as suggested by Barai and Weng (2011) in the study of CNT-based metal plasticity and also by Prasher et al. (2006) and Reinecke et al. (2008) in the context of thermal conductivity. In this approach, the composite is considered to consist of CNT-rich agglomerated regions embedded in a CNT-poor region. To calculate the effective electrical conductivity,

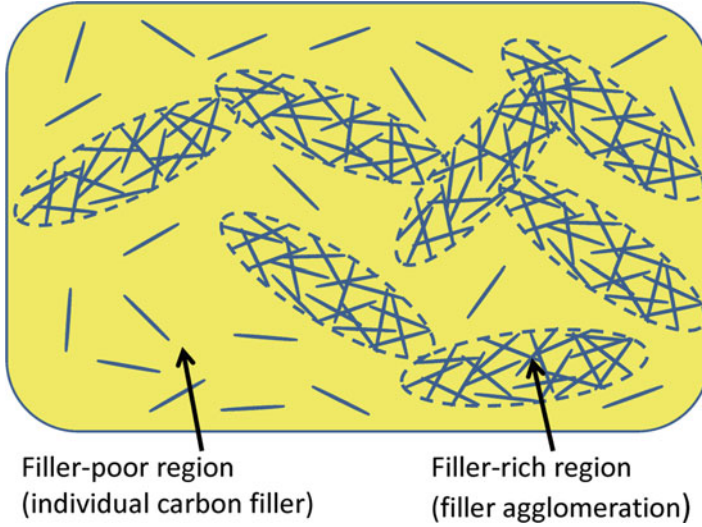


**Fig. 4.4** A schematic plot of the two-scale model of CNT- and graphene-based nanocomposites with filler agglomeration

the effective-medium approach is applied to the filler-rich and filler-poor regions at the smaller scale and then to the whole composite at the larger scale (Wang et al. 2015).

We will begin with establishing the two-scale morphology of the CNT and graphene-based nanocomposites with filler agglomeration. The typical microstructure of such composite is shown in Fig. 4.4. Inside the composite, some CNT or graphene fillers gather together to form the agglomerates, while others exist as individual fillers. Both kinds of fillers are taken to be homogeneously dispersed and randomly oriented in each region. To model such a morphology, we divide the entire volume of the composite into two—one is the filler-rich agglomerate and the other is the filler-poor region. The volume concentrations of the filler-rich and the filler-poor regions are denoted as  $c_R$  and  $c_P$ , respectively, so that

$$c_R + c_P = 1, \quad (4.18)$$

where subscript  $R$  stands for “rich” and  $P$  for “poor.” We assume that the agglomerates are also homogeneously dispersed and randomly oriented and have a shape that can be grossly represented by a spheroid, with an aspect ratio  $\alpha_R$ . Inside the agglomerate, there is a large amount of carbon fillers residing in the polymer matrix, with the volume concentrations,  $c_1^{(R)}$  and  $c_0^{(R)}$ , respectively, satisfying

$$c_1^{(R)} + c_0^{(R)} = 1, \quad (4.19)$$

where subscripts 1 and 0 stand for carbon fillers and the polymer matrix, respectively. We shall also represent the individual carbon filler by a spheroid with aspect ratio  $\alpha$ . In the filler-poor region, there are also carbon fillers and the polymer matrix, with the volume concentrations,  $c_1^{(P)}$  and  $c_0^{(P)}$ , respectively, such that

$$c_1^{(P)} + c_0^{(P)} = 1. \quad (4.20)$$

As a result, the total volume concentration of carbon fillers, denoted by  $c_1$ , is the sum of the filler concentration from both filler-rich and filler-poor regions, and so is the total volume concentration of the matrix,  $c_0$ . They satisfy

$$\begin{aligned} c_1 &= c_1^{(R)} c_R + c_1^{(P)} c_P, \\ c_0 &= c_0^{(R)} c_R + c_0^{(P)} c_P, \\ c_1 + c_0 &= 1. \end{aligned} \quad (4.21)$$

It is this  $c_1$  that represents the volume concentration of carbon fillers that is commonly measured in experiments. With these definitions, the dispersion state of carbon fillers can be fully described. However, we still need to know how they evolve as  $c_1$  increases. Here we choose to study the dependence of  $c_R$ ,  $c_1^{(R)}$ , and  $c_1^{(P)}$ , as the other three can be calculated from them. There are two basic requirements for  $c_R$ ,  $c_1^{(R)}$ , and  $c_1^{(P)}$ . The first one is that, if there are no carbon fillers in the composite, there should be no filler agglomerates and no individual filler inside the filler-poor region. In other words, when  $c_1 = 0$ , we must have  $c_R = 0$  and  $c_1^{(P)} = 0$ . The second one is that, if carbon fillers occupy the entire composite, then both the filler-rich and the filler-poor regions are completely filled. This implies that, when  $c_1 = 1$ , we must have both  $c_1^{(R)} = 1$  and  $c_1^{(P)} = 1$ .

We also need to know how graphene fillers are distributed into the graphene-rich and the graphene-poor regions. For this purpose, we introduce a parameter,  $a$  ( $0 \leq a \leq 1$ ), to represent the volume fraction of graphene inside the graphene-rich region out of the total amount of graphene; it satisfies

$$a = c_1^{(R)} c_R / c_1. \quad (4.22)$$

Essentially, the parameter  $a$  specifies how much of the total amount of carbon filler is allocated to the filler-rich region. We also need to specify the dependence of  $c_1^{(R)}$  on  $c_1$ . As the filler agglomerate tends to percolate earlier than the entire composite,  $c_1^{(R)}$  can be greater than the percolation threshold of the filler-rich region at low  $c_1$ . Hence when  $c_1 \rightarrow 0$ ,  $c_1^{(R)}$  doesn't need to start from 0 but can have a non-zero initial value, represented by another parameter  $b$ . But this  $c_1^{(R)}$  must grow to 1 when  $c_1 = 1$ . From these two requirements we assume a linear dependence on  $c_1$  for  $c_1^{(R)}$ , as

$$c_1^{(R)} = b + c_1 (1 - b). \quad (4.23)$$

Parameter  $b$  also lies between 0 and 1. When  $b = 0$ , we have  $c_1^{(R)} = c_1^{(P)} = c_1$ . So there is no distinction among the three and thus the composite is homogeneous. For an agglomerated composite, its  $b$  value has to be greater than 0, so that  $c_1^{(R)} > c_1$ . This implies that carbon fillers are more concentrated inside the filler-rich region, and its percolation condition is reached earlier than that of the overall nanocomposite. It should also be noted that it is the quantity,  $c_1^{(R)} c_R$ , that specifies the volume fraction of carbon fillers out of the total  $c_1$  to reside inside the agglomerates. When  $c_1 = 0$ , the volume fraction of the filler-rich region is zero, i.e.,  $c_R = 0$ . So even though  $c_1^{(R)} \neq 0$  in this situation, there is still no carbon filler in the “filler-rich” region or anywhere else.

With parameters  $a$  and  $b$ , we can then obtain the dependence of  $c_R$  and  $c_1^{(P)}$  on  $c_1$ , as

$$\begin{aligned} c_R &= \frac{a}{b + c_1(1 - b)} c_1, \\ c_1^{(P)} &= \frac{(1 - a)[b + c_1(1 - b)]}{-c_1 a + [b + c_1(1 - b)]} c_1. \end{aligned} \quad (4.24)$$

The dispersion state of carbon fillers is now completely specified by the two parameters,  $a$  and  $b$ . In the limiting case when  $a = 1$ , all fillers are allocated to the agglomerates and there is no  $c_1^{(P)}$ . When  $a = 0$ , we have  $c_R = 0$  and  $c_1^{(P)} = c_1$ , so the composite is completely specified by the filler-poor region. In both cases the two-scale composite is reduced to only one scale, making it back to a homogeneous composite. With Eqs. (4.23) and (4.24) representing the geometrical foundation of filler agglomeration, we have now fully established the two-scale morphology of CNT and graphene-based nanocomposites.

To evaluate the effective electrical conductivity, the effective-medium approach, as given in Eq. (4.10), is applied to the two scales. At the smaller scale of the filler-rich and filler-poor regions, phase 1 is identified as the individual carbon filler. It has transversely isotropic property with electrical conductivity  $\sigma_3$  in the normal direction and  $\sigma_1 = \sigma_2$  in the isotropic plane, S-tensor components  $S_{11}$  and  $S_{33}$  which are determined by its aspect ratio  $\alpha$  according to Eq. (4.8), and volume concentration  $c_1$  replaced by  $c_1^{(R)}$  (for the filler-rich region) or  $c_1^{(P)}$  (for the filler-poor region). Phase 0, on the other hand, is identified as the polymer matrix. It has isotropic electrical conductivity  $\sigma_0$ , S-tensor component  $1/3$  in all three directions, and volume concentration  $c_0$  replaced by  $c_0^{(R)}$  (for the filler-rich region) or  $c_0^{(P)}$  (for the filler-poor region). On the larger scale of the composite, phase 1 is identified as the filler agglomerates while phase 0 as the filler-poor region. In this case  $\sigma_3$  and  $\sigma_1$  become the overall electrical conductivity of the filler-rich region in the normal and in-plane direction;  $\sigma_0$  becomes the overall electrical conductivity of the filler-poor region;  $S_{11}$  and  $S_{33}$  are replaced by the S-tensor components of filler agglomerates,  $S_{11}^{(R)}$  and  $S_{33}^{(R)}$ , which are calculated from the aspect ratio of filler agglomerates,  $\alpha_R$ ; and lastly,  $c_1$  and  $c_0$  become  $c_R$  and  $c_P$ , respectively.

In our two-scale model, the calculation of effective electrical conductivity of the overall nanocomposite takes two steps. In the first place, in both filler-rich and filler-poor regions, carbon fillers are embedded in the polymer matrix (or more strictly speaking, both carbon fillers and the polymer matrix are embedded in the effective medium, as indicated by effective-medium approach). So we use Eq. (4.10) on the smaller scale to obtain the overall electrical conductivity of the filler-rich and filler-poor region, respectively. On the larger scale, it can be regarded that the filler agglomerates are embedded in the filler-poor region. Therefore, we take advantage of the properties of both regions to implement Eq. (4.10) once again, and the effective electrical conductivity of the overall composite,  $\sigma_e$ , can then be solved.

The percolation threshold will also be affected by the dispersion state of carbon fillers. By using the S-tensor of individual carbon filler, Eq. (4.16) can be used to determine the percolation threshold of the filler-rich region, with  $c_1^*$  identified as  $c_1^{(R)*}$ .  $c_1^{(R)*}$  is related to  $c_1^*$  of the overall composite through Eq. (4.23), such that

$$c_1^* = \frac{c_1^{(R)*} - b}{1 - b}, \quad \text{where} \quad c_1^{(R)*} = \frac{9S_{33} (1 - S_{33})}{-9S_{33}^2 + 15S_{33} + 2}. \quad (4.25)$$

Likewise, Eq. (4.16) can also be used to determine the percolation condition of the large-scale overall composite,  $c_R^*$ , by identifying the S-tensor as that of the filler agglomerate. This  $c_R^*$  is related to  $c_1^*$  of the composite through Eq. (4.24), such that

$$c_1^* = \frac{bc_R^*}{a - (1 - b)c_R^*}, \quad \text{where} \quad c_R^* = \frac{9S_{33}^{(R)} (1 - S_{33}^{(R)})}{-9S_{33}^{(R)2} + 15S_{33}^{(R)} + 2}, \quad (4.26)$$

where  $S_{33}^{(R)}$  is the S-tensor component of the filler agglomerate that depends on its aspect ratio,  $\alpha_R$ . For the overall nanocomposite to be in a percolated state, the percolation condition by individual carbon filler inside the filler-rich region as specified by Eq. (4.25) and the percolation condition by the large-scale agglomerates specified by Eq. (4.26) must both be satisfied. So it is the larger of the two  $c_1^*$  calculated from these two equations that represents the true percolation threshold of the nanocomposite. But in general it is the second one given by Eq. (4.26) that defines the percolation threshold as the first condition is easier to meet. It is clear from Eq. (4.26) that the percolation threshold  $c_1^*$  for the overall, large-scale composite depends on three parameters,  $a$ ,  $b$ , and  $\alpha_R$ . Parameter  $a$  specifies how much of the total amount of carbon fillers is allocated to the filler-rich agglomerates; parameter  $b$  specifies the volume fraction of carbon fillers inside the agglomerate,  $c_1^{(R)}$ ; and parameter  $\alpha_R$  specifies the shape of the agglomerates. All of them together describe the dispersion state of carbon fillers.



#### 4.2.4 The Interfacial Resistance

In this section we will consider the effect of imperfect interfaces on the effective electrical conductivity. So far we have assumed perfect interface condition between the two phases of CNT and graphene-based nanocomposites, but in real composite materials the interface condition can never be perfect. The effect of imperfect interfaces results in electrical resistance between two phases, which is the interfacial resistance. This makes the transport of electric current more difficult, so that without this additional consideration the calculated  $\sigma_e$  could be much higher than the actual value. To address this issue, we first consider the existence of a very thin spheroidal layer of interphase by adding a tiny thickness  $t$  to the semi-axes of the spheroidal CNT or graphene inclusion, with an electrical conductivity,  $\sigma_i^{\text{int}}$ . This layer is taken to surround the spheroidal inclusion, making it similar to a “thinly coated” inclusion. Due to the imperfect condition,  $\sigma_i^{\text{int}}$  is usually much lower than the intrinsic conductivity of carbon fillers,  $\sigma_i$ , so that it is reasonable to assume  $\sigma_i^{\text{int}}/\sigma_i \rightarrow 0$ . Compared to the radius of CNT  $R$ , or the thickness of the graphene  $\lambda$ ,  $t$  is taken to be diminishingly small and we intend to make it approach zero to turn the interphase into an interface. In the limiting case of diminishing thickness ( $t \rightarrow 0$ ), the “coated” inclusion and the original inclusion share the same shape, or the same S-tensor. This is a typical inclusion-matrix type of problem; therefore the M-T method is appropriate to calculate the overall electrical conductivity of the coated inclusion,  $\sigma_i^c$ , as

$$\sigma_i^c = \sigma_i^{\text{int}} \left[ 1 + \frac{\nu (\sigma_i - \sigma_i^{\text{int}})}{(1 - \nu) S_{ii} (\sigma_i - \sigma_i^{\text{int}}) + \sigma_i^{\text{int}}} \right], \quad (4.27)$$

where  $i = 1$  or  $3$  (no sum over  $i$  in  $S_{ii}$ ), denoting the transverse or axial direction. And  $\nu$  is the volume fraction of the original inclusion in the coated inclusion. For a CNT inclusion, by taking the limit  $t \rightarrow 0$ ,  $\nu$  can be written as

$$\nu = \left(\frac{R}{\alpha}\right) R^2 / \left[\left(\frac{R}{\alpha} + t\right) (R + t)^2\right] \approx 1 - \left(\frac{1}{\alpha} + 2\right) \frac{t}{R}. \quad (4.28)$$

Then, with the assumption  $\sigma_i^{\text{int}}/\sigma_i \rightarrow 0$ , Eq. (4.27) can be rewritten as

$$\sigma_i^c = \frac{\sigma_i}{1 + \rho_i \sigma_i S_{ii} (1/\alpha + 2)/R}. \quad (4.29)$$

Similarly, for a graphene inclusion,  $\nu$  is expressed in terms of  $\lambda$  and  $t$ , as

$$\nu = \frac{\lambda}{2} \left(\frac{\lambda}{2\alpha}\right)^2 / \left[\left(\frac{\lambda}{2} + t\right) \left(\frac{\lambda}{2\alpha} + t\right)^2\right] \approx 1 - (2 + 4\alpha) \frac{t}{\lambda}. \quad (4.30)$$

and Eq. (4.27) is then rewritten as

$$\sigma_i^{(c)} = \frac{\sigma_i}{1 + \rho_i \sigma_i S_{ii} (2 + 4\alpha) / \lambda}. \quad (4.31)$$

In Eqs. (4.29) and (4.31),  $\rho_i = \lim_{\sigma_i^{\text{int}}/\sigma_i \rightarrow 0, t \rightarrow 0} t/\sigma_i^{\text{int}}$  stands for the interfacial resistivity in the axial or transverse direction. For simplicity, it's convenient to take the property of interface to be isotropic, so that  $\rho_i = \rho$ . This result is also consistent with the Kapitza resistance in thermal conductivity derived by Nan et al. (1997) and Duan and Karihaloo (2007). This electrical conductivity of coated CNT,  $\sigma_i^c$ , can then be used to replace the original  $\sigma_i$  in Eq. (4.10) of the effective-medium approach to calculate the effective electrical conductivity of imperfectly bonded nanocomposites. In this way, the effect of interfacial resistance has been incorporated into our model.

#### 4.2.5 The Tunneling-Assisted Interfacial Conductivity

The interfacial resistivity  $\rho$  is an intrinsic property of the interface between carbon fillers and the polymer matrix, and we denote its intrinsic value as  $\rho_0$ . This quantity contributes to the overall electrical conductivity of the coated CNT,  $\sigma_i^c$ , through Eq. (4.29) or (4.31). However as the inclusion volume concentration  $c_1$  increases,  $\rho$  cannot remain constant at  $\rho_0$ . Electron hopping from one carbon filler to the surface of another one can lead to enhanced electrical conductivity. This phenomenon, that electrons can directly pass through insulating polymer from one CNT to an adjacent one, is the quantum mechanical electron tunneling effect. The outcome is a higher interfacial conductivity, or conversely, a lower interfacial resistivity. It plays an essential role the electrical conduction process, but it is also difficult to analyze due to its complex quantum mechanical nature.

In our continuum model we take this tunneling effect as a statistical process that depends on the volume concentration of carbon fillers. In establishing a probabilistic function, we note that, at dilute filler concentration, the distance between carbon fillers is large and there is little tunneling possibility, so there is a large interfacial resistivity, but around the percolation threshold  $c_1^*$ , the conductive networks begin to build up and the overall distance between carbon fillers is greatly reduced. As a consequence electron tunneling activity starts to become very intense and  $\rho$  begins to decrease. After  $c_1^*$ , fillers will get even closer, and thus tunneling effect will continue to be at a very high level, so that  $\rho$  will stay very low. It turns out that Cauchy's probabilistic model is particularly suited to describe this phenomenon. We will incorporate Cauchy's cumulative distribution function,  $F$ , which can signify the dramatic increase of interfacial conductivity near  $c_1^*$ , to describe this tunneling effect. This function is given by

$$F(c_1; c_1^*, \gamma) = \frac{1}{\pi} \arctan\left(\frac{c_1 - c_1^*}{\gamma}\right) + \frac{1}{2}, \quad (4.32)$$

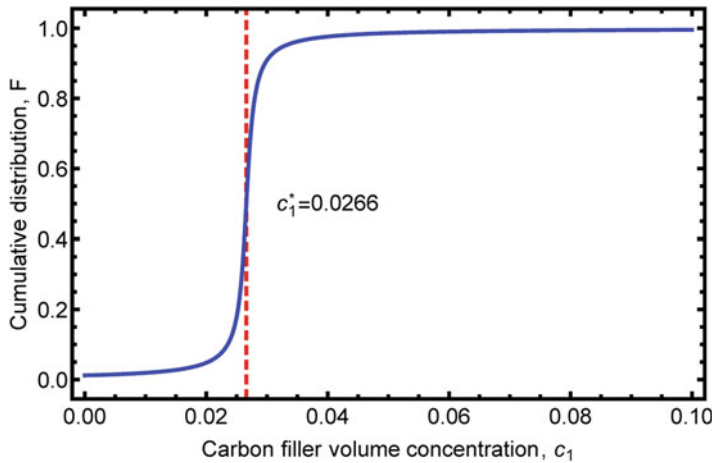


**Fig. 4.5** The illustration of Cauchy's cumulative distribution function in Eq. (4.32), showing an increasing tunneling activity near the percolation threshold

where  $\gamma$  is a scale parameter denoting the rate of change for function  $F$  around  $c_1 = c_1^*$ . The nature of function  $F$  is illustrated in Fig. 4.5 with  $c_1^* = 0.0266$  and  $\gamma = 0.001$ . It displays a sharp increase around  $c_1^*$  and continues to hold afterward. With function  $F$ , the decrease of interfacial resistivity  $\rho$  from  $\rho_0$  as  $c_1$  increases can be described by

$$\rho = \rho(c_1) = \rho_0 [F(1; c_1^*, \gamma) - F(c_1; c_1^*, \gamma)] / [F(1; c_1^*, \gamma) - F(0; c_1^*, \gamma)]. \quad (4.33)$$

This  $c_1$ -dependent  $\rho$  is the tunneling-assisted interfacial resistivity, which returns to  $\rho = \rho_0$  at  $c_1 = 0$  and  $\rho = 0$  at  $c_1 = 1$ . The nature of its variation is illustrated in Fig. 4.6 which shows a drastic decrease of interfacial resistivity around  $c_1^*$ . This tunneling-assisted interfacial resistivity  $\rho(c_1)$  now should replace the original interfacial resistivity in Eqs. (4.29) and (4.31) to calculate the electrical conductivity of the coated inclusion  $\sigma_i^c$ , which in turn will replace  $\sigma_i$  in Eq. (4.11) for the effective electrical conductivity,  $\sigma_e$ , of the overall nanocomposite. In this way, the influence of electron tunneling effect has been incorporated into our continuum model via the tunnel-assisted interfacial resistivity,  $\rho(c_1)$ . Up to this point we have completed the development of our continuum model for CNT and graphene-based nanocomposites. We now present some calculated results and make comparisons with experimental data.

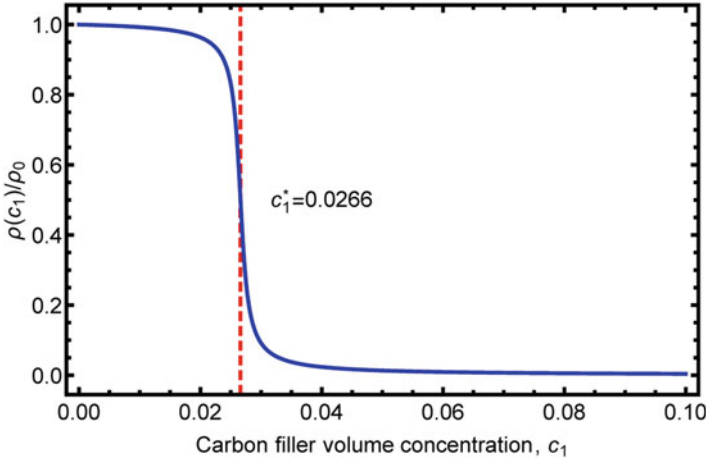


**Fig. 4.6** The illustration of the tunneling-assisted interfacial resistivity in Eq. (4.33), which leads to a sharp drop in resistivity near the percolation threshold

## 4.3 Results and Discussion

### 4.3.1 The Electrical Conductivity of CNT Nanocomposites

To verify our continuum composite model, we take two steps to study the experimental data of the electrical conductivity of CNT nanocomposites and agglomerated graphene nanocomposites. In the first step, the composite is taken to be homogeneous. We use the effective-medium approach with interfacial resistance and tunneling-assisted interfacial conductivity to study two sets of experimental data by Ngabonziza et al. (2011) and McLachlan et al. (2005) showing notable percolation phenomena. The first set of data involved multi-walled CNTs in the polyimide matrix, while the second set was with single-walled CNTs and also the polyimide matrix. The intrinsic electrical conductivity of CNTs and the matrix are both given in the original papers and are listed in Table 4.1. In our calculations the anisotropic constant  $m$ , in  $\sigma_1 = m\sigma_3$ , for the CNT inclusion is assumed to be 0.001 at this moment. All other relevant material constants used in the calculations are also listed in Table 4.1.

#### 4.3.1.1 The Effective Electrical Conductivity of the Coated CNT

With Cauchy's cumulative distribution function  $F$ , we then use Eq. (4.29) to calculate the increase of the effective electrical conductivity of the coated CNT,  $\sigma_i^c$ , as  $c_1$  increases, to reflect the contribution from the probabilistic electron tunneling process. The results with these two sets of experimental data are shown in Fig. 4.7a, b, respectively, where the upper blue curves are for the axial electrical conductivity

**Table 4.1** Physical values used in the calculation of the effective electrical conductivity of CNT nanocomposites

Physical values	Ngabonziza et al. 2011	McLachlan et al. 2005
$\sigma_0$	$2.0 \times 10^{-8}$ S/m	$5.5 \times 10^{-15}$ S/m
$\sigma_3$	$1.943 \times 10^4$ S/m	$8.9 \times 10^3$ S/m
$\sigma_3/\sigma_0$	$9.715 \times 10^{11}$	$1.8 \times 10^{18}$
$m$	$10^{-3}$	$10^{-3}$
Percolation threshold	0.0266	0.0005
Aspect ratio $\alpha$	21	213
CNT radius $R$	5 nm	5 nm
Interfacial resistivity $\rho_0$	$4.82 \times 10^{-8}$ m <sup>2</sup> /S	$7.16 \times 10^{-4}$ m <sup>2</sup> /S
Scale parameter $\gamma$	0.003	0.0003

and the lower red ones for the transverse electrical conductivity. These two sets of data have substantially different percolation thresholds, one at 0.0266 and the other at 0.0005. So the initial, nearly horizontal portion spans over a wider range of  $c_1$  in the first set, but following the percolation threshold, both curves display a notable increase due to the stronger electron tunneling effect associated with the conductive network formation.

This characteristic can be made more apparent if we rewrite Eq. (4.29) as

$$\sigma_i^c = \frac{1}{1/\sigma_i + \rho(c_1) S_{ii} (1/\alpha + 2) / R}. \quad (4.34)$$

It can be observed that, when  $c_1 < c_1^*$ , the numerical value of  $\rho(c_1) S_{ii} (1/\alpha + 2) / R$  is much larger than  $1/\sigma_i$ . So in this case the latter can be neglected and we have, approximately,  $\sigma_i^c = R / [\rho(c_1) S_{ii} (1/\alpha + 2)]$ , which means that  $\sigma_i^c$  is now mainly controlled by the interfacial resistivity, rather than the intrinsic electrical conductivity of CNT. As such, the several-orders-of-magnitude difference between the axial conductivity  $\sigma_3^c$  and the transverse conductivity  $\sigma_1^c$  is only a result of the different components in the S-tensor. S-tensor characterizes the geometric property of CNT, which has a prolate spheroidal shape. Comparing Fig. 4.7a, b, it can be further pointed out that the higher aspect ratio in the second data set also leads to larger difference between  $\sigma_3^c$  and  $\sigma_1^c$ . Therefore we can conclude that the geometry of CNT inclusions plays a very important role in the anisotropy of  $\sigma_i^c$ .

#### 4.3.1.2 The Effective Electrical Conductivity of CNT Nanocomposites

With the  $c_1$ -dependent  $\sigma_i^c$  to replace the original  $\sigma_i$  in Eq. (4.11), the effective electrical conductivity of CNT nanocomposites,  $\sigma_e$ , can be calculated as a function of CNT concentration  $c_1$ . The results are plotted in Figs. 4.8 and 4.9, respectively, that correspond to the experiment results of Ngabonziza et al. (2011) and McLachlan et al. (2005). In both figures the highest red curve represents the calculated result

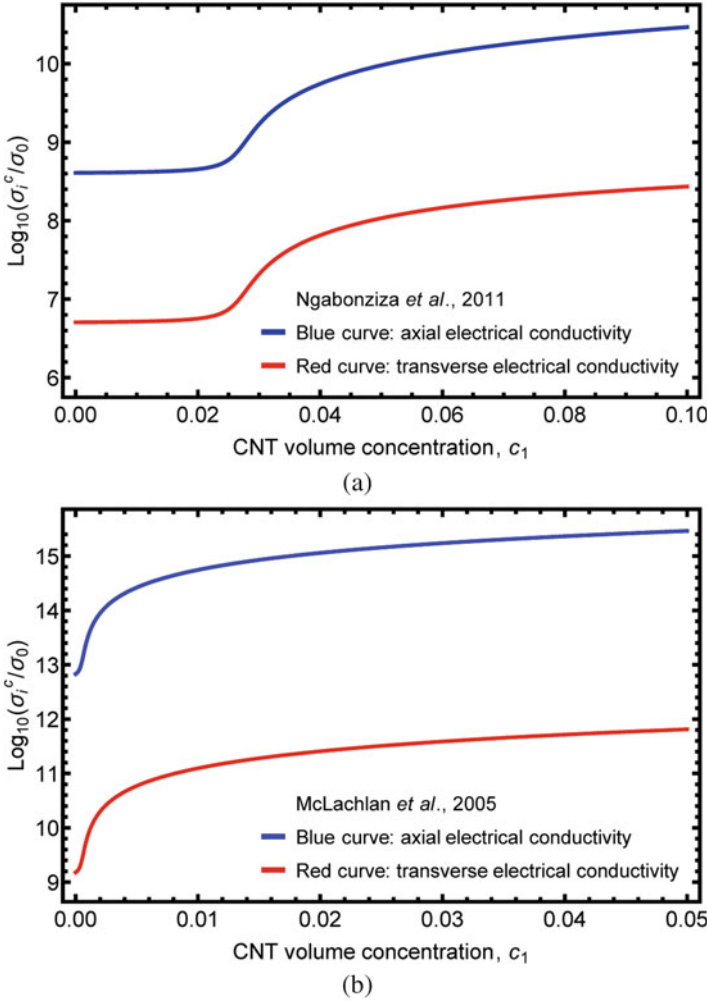


**Fig. 4.7** The electrical conductivity of coated CNT inclusion with the consideration of the interfacial resistance and tunneling-assisted interfacial conductivity: (a) by Ngabonziza et al. (2011) data and (b) by McLachlan et al. (2005) data

under the assumption of perfect interface between CNT inclusions and the matrix. It is seen that, without accounting for the interfacial resistance, the theoretical predictions are substantially higher than the experimental data. The lowest black curve in each figure represents the case in which the interfacial resistance is included, but the interfacial resistivity  $\rho$  is regarded as a constant value  $\rho_0$ . This curve is seen to be lower than the experimental data, especially after percolation threshold. The middle blue curve represents the case in which  $\rho$  is modified to  $\rho(c_1)$  according to Eq. (4.33) with the consideration of the additional contribution from

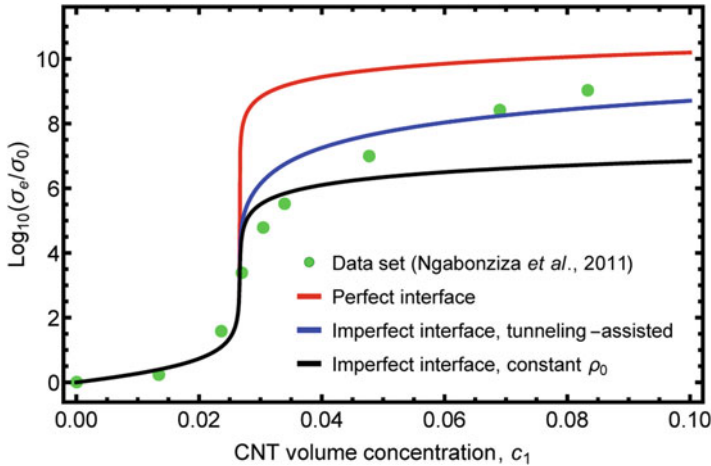


**Fig. 4.8** The effective electrical conductivity of CNT nanocomposites with Ngabonziza et al. (2011) data

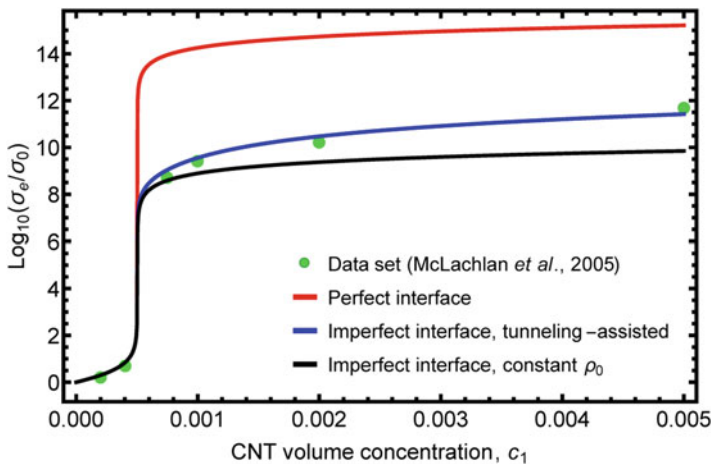


**Fig. 4.9** Effective electrical conductivity of CNT nanocomposites with McLachlan et al. (2005) data

the effect of tunneling-assisted interfacial conductivity. And this curve gives the best predictions for the experimental data. This study clearly confirms the view that the effect of imperfect interface is important and that the tunneling-assisted increase in interfacial conductivity is also a critical component of the theory. It is the combination of the effective-medium approach, interfacial resistance, and tunneling-assisted interfacial conductivity that eventually gives rise to a complete theory for the effective electrical conductivity of CNT nanocomposites.

### 4.3.1.3 The Effect of CNT Anisotropy

Now with the theory established, we can examine the effect of CNT anisotropy on the effective electrical conductivity. In our previous analysis, the results were obtained based on the assumed value of  $m = 10^{-3}$ . In fact while the transverse electrical conductivity of CNT is known to be several orders of magnitude lower than the axial one, the precise value of  $m$  is not clear yet. Thus further parametric studies are needed to clarify its effect. So we again use the first set of parameters listed in Table 4.1 for the experimental data of Ngabonziza et al. (2011) and consider four cases from isotropic to transversely isotropic, with  $m = 1, 10^{-3}, 10^{-8}$ , and 0, with the last one meaning that there is only axial electrical conductivity. The results are displayed in Fig. 4.10. From this figure we can immediately conclude that the effective electrical conductivity of overall composite is not sensitive to the value of  $m$ . Although the transverse electrical conductivity of CNT is lower than its axial one, it still has to be much higher than that of the polymer matrix. So far we have not seen any direct measurement on  $\sigma_1$  for CNT, but for graphite sheets the electrical conductivity in the basal plane has been reported to be about 2–3 orders of magnitude higher than that along the normal direction. In this regard the value of  $m$  is most likely to lie within the range of  $10^{-3} \sim 10^{-2}$ , and our assumed value of  $10^{-3}$  can be so justified.

### 4.3.1.4 The Effective Electrical Conductivity with a Totally Insulating Matrix

In CNT nanocomposites, electric current can flow from CNT inclusions to the matrix, or from one CNT to another one in contact. Both ways, plus the direct

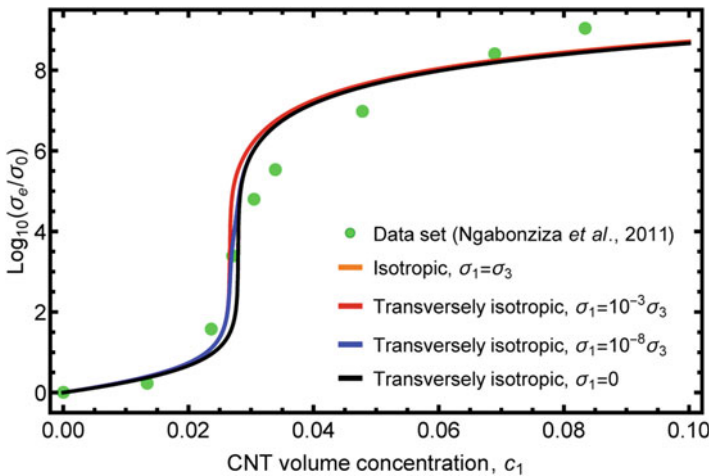


**Fig. 4.10** The effect of CNT anisotropy on the overall electrical conductivity. The orange isotropic curve is entirely overlapped by the red transversely isotropic curve because of their insignificant difference



electron tunneling from one CNT to another, can all contribute to the overall electrical conductivity. So even when the polymer matrix is totally insulating ( $\sigma_0 = 0$ ), a viable continuum composite model should still be able to deliver a non-zero  $\sigma_e$  from the last two mechanisms. In fact, even without the electron tunneling process, direct contact between CNT inclusions should still provide a conductive pathway for current flows, and thus the overall electrical conductivity should still exist. Such a capability, however, is lost in both the M-T method and the PCW model, because in both cases each CNT inclusion must be embedded in the polymer matrix. This can be seen from Eq. (4.11) that, if  $\sigma_0 = 0$ , the effective electrical conductivity will be  $\sigma_e = 0$  (to see this, multiply  $\sigma_0$  on both sides of the equation). To test such a capability for the effective-medium approach, we take Eq. (4.10) to solve for  $\sigma_e$  under the insulating matrix condition. As has been discussed before, initially when  $c_1$  is very low, all coefficients A, B, and C in Eq. (4.15) are positive, so there are two negative roots, which should be rejected since the electrical conductivity must be positive. Only when  $c_1 > c_1^*$ , coefficient C becomes negative, and there is one positive root, which is the effective electrical conductivity we want to solve. The condition of  $C = 0$  is a critical point where the root is  $\sigma_e = 0$ . This analysis indicates that, when  $c_1 < c_1^*$ , since at this stage all CNT inclusions are isolated by the insulating matrix, there is no overall electrical conductivity. And when  $c_1 \geq c_1^*$ , the nanocomposite starts to give a non-negative electrical conductivity due to the formation of the conductive network. With the first set of constants taken from Table 4.1, the calculated  $\sigma_e$  from  $c_1 = c_1^*$  to  $c_1 = 0.1$  is shown in Fig. 4.11. A drastic increase of electrical conductivity is observed near the percolation threshold.

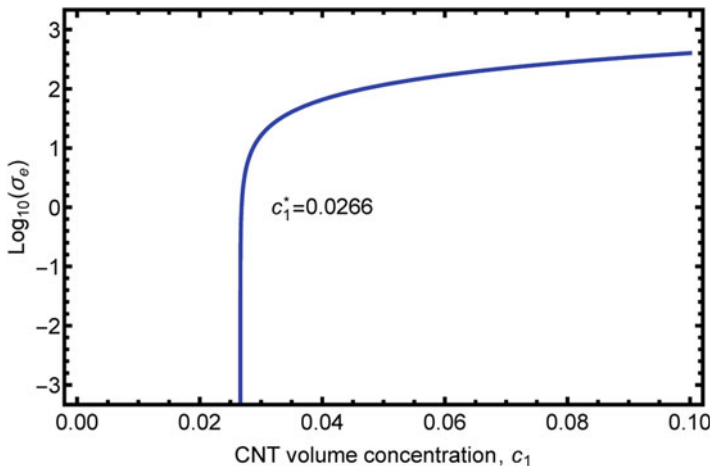


**Fig. 4.11** The examination of the effective-medium approach for the effective electrical conductivity of a composite with a totally insulating matrix

### 4.3.2 The Electrical Conductivity of Agglomerated Graphene Nanocomposites

In the last section our model has been successfully applied to study the electrical conductivity of homogeneous CNT nanocomposites. In this section we will focus on its capability to deal with nanocomposites with filler agglomeration, and we do so by demonstrating that a set of experimental data reported by Tkalya et al. (2014) for the electrical conductivity of agglomerated graphene/polystyrene nanocomposites can be well captured by this theory.

This set of data consists of 4 samples of graphene nanocomposites with different degrees of filler agglomeration, which is reproduced in Fig. 4.12. Note that the electrical conductivity has the unit of S/m, and is shown in logarithmic scale. Among them sample B has the highest percolation threshold of  $c_1^* = 0.023$ , followed by samples A-HE, A-LC, and A with  $c_1^* = 0.015$ , 0.012, and 0.010 (note that the original data are in wt.%, and they have been converted to vol.% by considering the density of graphene is twice of that of polystyrene). It is also reported that the different degrees of graphene agglomeration are due to different processing routes. The graphene fillers in sample B are produced by the liquid-phase exfoliation of graphite, which have the most dispersed distribution. In the other three samples, graphene fillers are prepared by the thermal reduction of graphite oxide but with different amount of energy provided during the sonication process. Samples A and A-LC are more agglomerated than sample A-HE, which is in line with the fact that more energy was supplied to sample A-HE during the sonication process. In addition sample A is slightly more agglomerated than sample A-LC, making it the most agglomerated sample among the four. Based on these observations, we assume

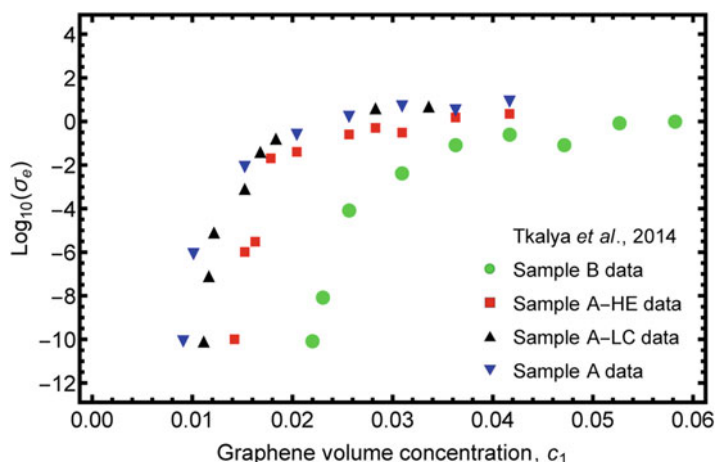


**Fig. 4.12** The experimental data on the electrical conductivity of 4 samples of graphene nanocomposites with various degrees of filler agglomeration, reproduced from Tkalya et al. (2014)

**Table 4.2** Physical values used in the calculations for agglomerated graphene nanocomposite samples B, A-HE, A-LC, and A. The last column gives the percolation threshold for the idealized spherical agglomerates

	Sample A	Sample A-LC	Sample A-HE	Sample B	Spherical agglomerates
Parameter $a$	0.9	0.8	0.9	...	0.7
Parameter $b$	0.05	0.08	0.05	...	0.05
Percolation threshold (%)	1.01	1.16	1.52	2.30	4.35
Aspect ratio of agglomerate $\alpha_R$	0.1241	0.0728	0.1399	...	1.0
Thickness of agglomerate $\lambda$ (nm)	50	50	50	...	50
Initial interfacial resistivity $\rho_0$ (m <sup>2</sup> /S)	$5 \times 10^{-8}$	$1 \times 10^{-7}$	$6 \times 10^{-7}$	$5 \times 10^{-7}$	$5 \times 10^{-7}$
Scale parameter $\gamma$	0.03	0.003	0.01	0.001	0.01

that the amount of graphene agglomeration in sample B is negligible and that the degree of graphene agglomeration increases from sample A-HE, to A-LC, and to A.

In our numerical computations, the in-plane electrical conductivity of graphene is taken to be  $\sigma_1 = 8.32 \times 10^4$  S/m, which is adopted from Stankovich et al. (2006) (they gave a range of  $10^{4.92 \pm 0.52}$  S/m), and the electrical conductivity of polystyrene is taken to be  $\sigma_0 = 6.09 \times 10^{-12}$  S/m, from Srivastava and Mehra (2008). The anisotropic constant  $m$ , in  $\sigma_1 = m\sigma_3$ , is taken to be  $10^3$  since normal electrical conductivity is weaker for graphene. Other material parameters used here include the aspect ratio of graphene  $\alpha = 0.0136$ , the thickness of graphene  $\lambda = 5$  nm, the initial interfacial resistivity  $\rho_0 = 5 \times 10^{-7}$  m<sup>2</sup>/S, and scale parameter  $\gamma = 0.001$ . On the larger scale of the composite consisting of graphene-rich agglomerates and graphene-poor region, the constants used are sample dependent and listed in Table 4.2. Note that the listed  $\alpha_R$ ,  $\lambda$ , and  $\rho_0$  in Table 4.2 pertain to this large-scale property. With these constants, we now show the calculated results.

#### 4.3.2.1 Homogeneously Dispersed Graphene Nanocomposites: Sample B

First we consider the sample B data, which are reproduced in Fig. 4.13. This set of data has a reported percolation threshold of  $c_1^* = 0.023$ , which can be directly calculated from Eq. (4.16) with the aspect ratio  $\alpha = 0.0136$ , since this sample has negligible filler agglomerations. We make an initial calculation for the overall electrical conductivity by assuming perfect interfaces (with  $\rho = 0$ , or  $\sigma_i^{(c)} = \sigma_i$ ). The effective electrical conductivity can be obtained from Eq. (4.10). The calculated result is shown in red line in Fig. 4.13. The comparison between this curve and the experimental data clearly indicates that the calculated electrical conductivity is

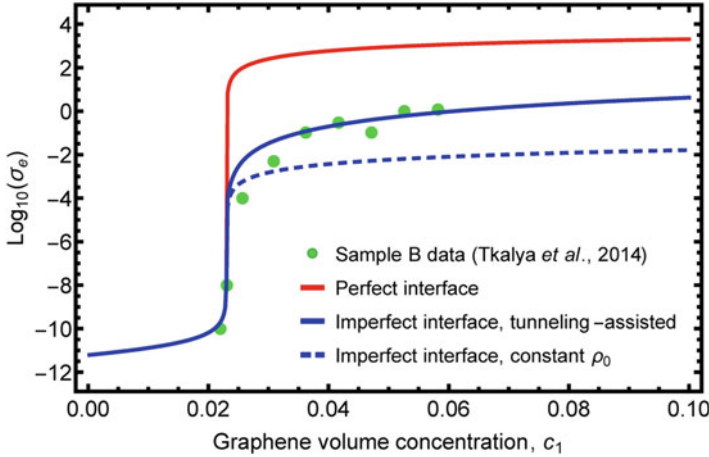


**Fig. 4.13** The theoretical curves for sample B data with perfect and imperfect interfaces

substantially higher than the test data. This is also an indication that the interface condition between graphene and polystyrene cannot be perfect.

In order to understand the effect of imperfect interfaces, we then use the constant interfacial resistivity,  $\rho = \rho_0$ , to make the calculation. The calculated conductivity is shown in the dashed blue line. When compared with the perfect interface curve, this result clearly shows a substantial drop to an order that is closer to the test data. But the trend of this curve is seen to stay relatively flat after percolation threshold. This is an indication that, without accounting for the additional contribution from the tunneling-assisted interfacial conductivity, the theoretical results become too low, especially after the percolation condition has been reached. When this tunneling effect is implemented through  $\rho(c_1)$  in Eq. (4.33), we can see a continuous gain in effective electrical conductivity as shown in the blue line. The outcome is a curve with an added slope, and the theory is then in very close agreement with the experimental data. This consideration strongly points to the need of an imperfect interface with a tunneling-assisted interfacial conductivity.

#### 4.3.2.2 Agglomerated Graphene Nanocomposites: Sample A-HE, A-LC, and A

We now use the two-scale composite model to study the effect of filler agglomeration on the percolation threshold and overall electrical conductivity in samples A-HE, A-LC, and A. These three samples were reported to have an increasing degree of agglomeration, respectively. Their experimental data are reproduced in Figs. 4.14, 4.15, and 4.16, along with theoretical results from the two-scale effective-medium approach. In each case parameters  $a$  and  $b$  and the aspect ratio of graphene-rich agglomerates,  $\alpha_R$ , are all involved in the calculation.

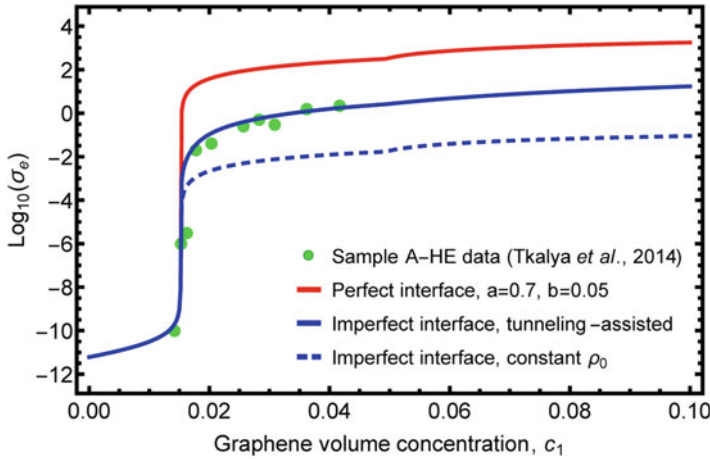


Fig. 4.14 The theoretical curves for sample A-HE data with perfect and imperfect interfaces

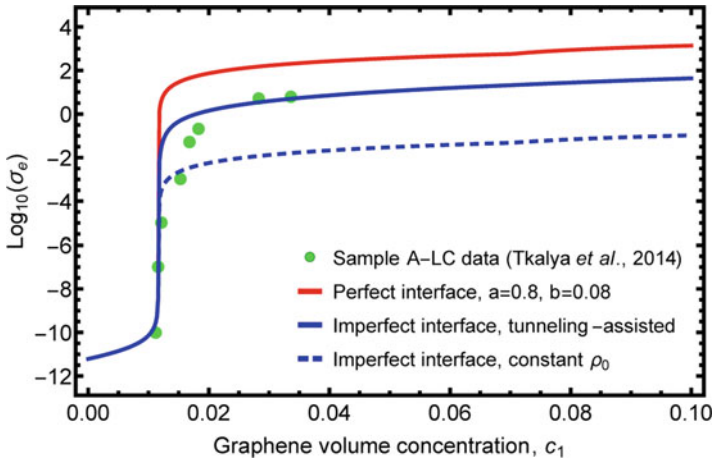


Fig. 4.15 The theoretical curves for sample A-LC data with perfect and imperfect interfaces

With the constants listed in Table 4.2, the calculated results for these three samples are also plotted in Figs. 4.14, 4.15, and 4.16. As with Fig. 4.13, the red line in each figure represents the calculated conductivity under the assumption of a perfect interface. The three red curves are seen to be notably higher than their respective experimental data. By implementing a constant interfacial resistivity,  $\rho = \rho_0$ , the calculated conductivity, shown in each dashed blue line, is significantly reduced. These curves, however, all appear to stay relatively flat after the percolation threshold. It is only when the tunneling-assisted interfacial conductivity is also implemented into the interface model can all the reported experimental data be well captured.

In passing it is also noted that there is a kink in the red curve in Fig. 4.14 around  $c_1 = 0.05$ , and so is in Fig. 4.15 around  $c_1 = 0.07$ . This slight increase is

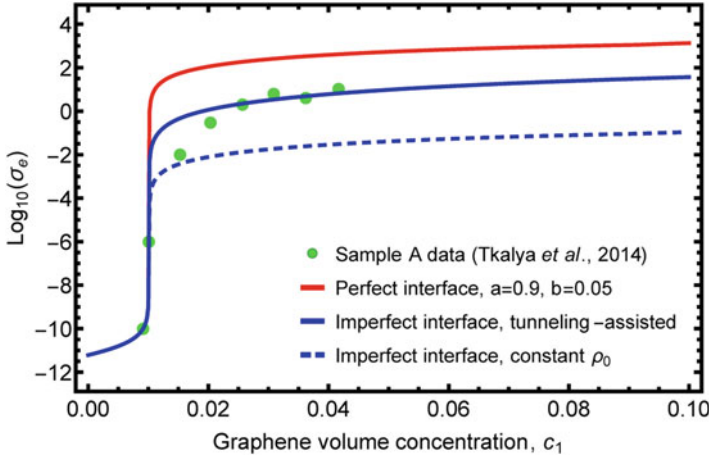


Fig. 4.16 The theoretical curves for sample A data with perfect and imperfect interfaces

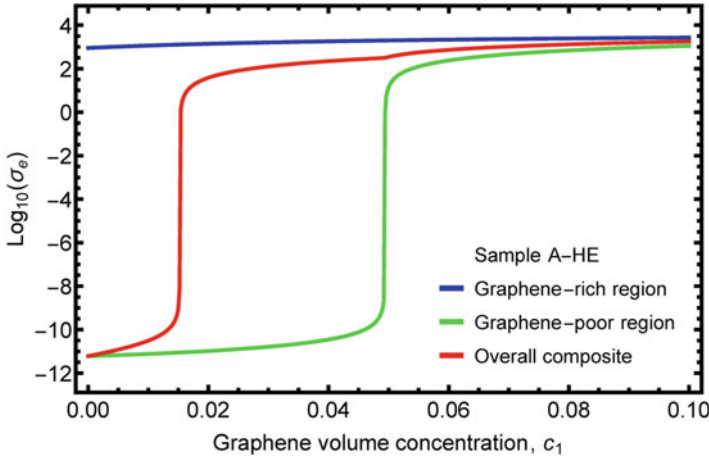


Fig. 4.17 The effective electrical conductivity of the graphene-rich and graphene-poor regions and the overall composite for sample A-HE

not an artifact of the computational results; it is due to the onset of percolation in the graphene-poor region. To reveal this phenomenon, we plot the effective electrical conductivity of the graphene-rich, and graphene-poor region, and the overall composite altogether in Fig. 4.17. It is clear that the graphene-rich region has been percolated since the beginning, and the graphene-poor region starts to percolate at the highest graphene concentration. The overall composite has the contributions from both two regions, so it has low electrical conductivity in the beginning, but it percolates earlier than the graphene-poor region.

### 4.3.2.3 The Role of Agglomerate Shape on the Percolation Threshold

The preceding discussions have suggested that filler agglomeration has the primary effect on the percolation threshold, and that interface conditions control the level of overall conductivity post percolation. In the past, it is often said that filler agglomeration tends to increase the percolation threshold, but we have proved and the discussed experiment has also shown that filler agglomeration can decrease the percolation threshold. This is a welcome consequence as high conductivity can be achieved at even lower graphene loading. But it cannot be concluded that graphene agglomeration will always lower the percolation threshold. The percolation threshold  $c_1^*$ , as shown in Eqs. (4.2) and (4.26), is seen to depend on the three parameters,  $a$ ,  $b$ , and  $\alpha_R$ . The first two specify the dispersion state of graphene in the agglomerates, whereas the third one defines the agglomerate shape. For the percolation threshold to decrease, the shape has to be sufficiently oblate (or prolate). If the shape is very rounded or becomes spherical, such a desirable outcome cannot be expected. To show such an effect, we have taken  $\alpha_R = 1$  while retaining the other parameters used in the calculation of A-HE to determine the corresponding percolation threshold. The newly calculated value is  $c_1^* = 0.044$ , which is higher than the percolation threshold of sample B, at  $c_1^* = 0.023$ . This value is listed in the last column of Table 4.2. So it is possible that the percolation threshold increases with spherical or more rounded agglomerates.

To be sure, the choice of a spherical shape for the agglomerates,  $\alpha_R = 1$ , does not guarantee that the calculated percolation threshold will always be higher than  $c_1^* = 0.023$ ; it also depends on the dispersion state represented by parameters  $a$  and  $b$ . This can be seen from the consideration of the percolation condition represented by Eq. (4.26). When  $\alpha_R = 1$ , that is, when  $c_R^* = 1/3$ , we have  $c_1^* = b/[3a - (1 - b)]$ . Therefore in order to have  $c_1^* > 0.023$ , it requires  $b/[3a - (1 - b)] > 0.023$  or  $b > 0.0235(3a - 1)$ , which is 0.026 when  $a = 0.7$ . From the last column of Table 4.2, the value of  $b$  is 0.05, which is indeed higher than 0.026; therefore the percolation threshold is higher than 0.023. If, instead, a value of  $b < 0.026$  is chosen, the overall percolation threshold would become lower than that of the homogeneously dispersed nanocomposites.

It is evident that the dispersion parameters  $a$  and  $b$ , and the agglomerate aspect ratio,  $\alpha_R$ , all contribute to the final percolation threshold,  $c_1^*$ , of the agglomerated graphene nanocomposites.

## 4.4 Conclusions

In this chapter, we have developed a continuum composite model to determine the effective electrical conductivity and percolation threshold of CNT and graphene-based nanocomposites. The theoretical framework of our model consists of four major components: (1) the effective-medium approach under perfect interface condition, (2) a two-scale model to account for the effect of filler agglomeration, (3) a diminishing layer of imperfect interface with an interfacial resistivity, and

(4) a statistical function to characterize the increase of interfacial conductivity due to electron tunneling effect. The outcome is a simple and widely useful model that can cover the nanocomposite with perfect and imperfect interfaces, as well as homogeneous and inhomogeneous filler distribution.

Our theories start with the effective-medium approach, which serves as the fundamental equation for the effective electrical conductivity of two-phase CNT and graphene-based nanocomposites. This equation also directly leads to the derivation of percolation threshold. To account for the effect of filler agglomeration, we then establish the two-scale model which divides the whole composite into filler-rich and filler-poor regions. The effective-medium approach is applied to the two-scale composite morphology by first determining the electrical conductivity of the filler-rich and the filler-poor regions and subsequently using their results to determine the overall electrical conductivity of the nanocomposite. Furthermore, the interfacial resistance and tunneling-assisted interfacial resistivity are incorporated in the model to cover the effect of imperfect interfaces and electron tunneling.

We have demonstrated that this model could successfully capture the quantitative behavior of two sets of experimental data of the electrical conductivity of homogeneous CNT nanocomposites. We also studied a set of experimental data of the agglomerated graphene nanocomposites to verify the applicability of our two-scale composite model. In this process, we have further shown how the imperfect interfaces lower the overall electrical conductivity and how the additional tunneling-assisted interfacial conductivity significantly brings it up after the percolation threshold. In addition, we have used the developed model to study the effect of the anisotropic electrical conductivity of carbon fillers in the axial and transverse directions and proved that this effect is insignificant. We have also proved that, even with a perfectly insulating matrix, the effective-medium approach is still capable of delivering non-zero electrical conductivity for the overall nanocomposites after the percolation threshold. In the end we have discussed how the percolation threshold can be influenced by the dispersion state of carbon fillers, as well as the shape of filler agglomerates.

**Acknowledgment** This work was supported by the US National Science Foundation, Mechanics of Materials Program, under grant CMMI-1162431.

## References

- Aguilar, J., Bautista-Quijano, J., Avilés, F.: Influence of carbon nanotube clustering on the electrical conductivity of polymer composite films. *Express Polym Lett.* **4**, 292–299 (2010)
- Allen, M.J., Tung, V.C., Kaner, R.B.: Honeycomb carbon: a review of graphene. *Chem. Rev.* **110**, 132–145 (2010)
- Balberg, I., Binenbaum, N., Wagner, N.: Percolation thresholds in the three-dimensional sticks system. *Phys. Rev. Lett.* **52**, 1465–1468 (1984)
- Bao, W.S., Meguid, S.A., Zhu, Z.H., Weng, G.J.: Tunneling resistance and its effect on the electrical conductivity of carbon nanotube nanocomposites. *J. Appl. Phys.* **111**, 093726 (2012)
- Bao, W.S., Meguid, S.A., Zhu, Z.H., Pan, Y., Weng, G.J.: Effect of carbon nanotube geometry upon tunneling assisted electrical network in nanocomposites. *J. Appl. Phys.* **113**, 234313 (2013)
- Barai, P., Weng, G.J.: A theory of plasticity for carbon nanotube reinforced composites. *Int. J. Plast.* **27**, 539–559 (2011)



- Bauhofer, W., Kovacs, J.Z.: A review and analysis of electrical percolation in carbon nanotube polymer composites. *Compos. Sci. Technol.* **69**, 1486–1498 (2009)
- Benveniste, Y.: A new approach to the application of Mori-Tanaka's theory in composite materials. *Mech. Mater.* **6**, 147–157 (1987)
- Bruggeman, D.A.G.: Calculation of various physics constants in heterogenous substances I Dielectricity constants and conductivity of mixed bodies from isotropic substances. *Ann. Phys.* **24**, 636–664 (1935)
- Budiansky, B.: On the elastic moduli of some heterogeneous materials. *J. Mech. Phys. Solids.* **13**, 223–227 (1965)
- Castañeda, P.P., Willis, J.R.: The effect of spatial distribution on the effective behavior of composite materials and cracked media. *J. Mech. Phys. Solids.* **43**, 1919–1951 (1995)
- Chatterjee, A.P.: A percolation-based model for the conductivity of nanofiber composites. *J. Chem. Phys.* **139**, 224904 (2013)
- Deng, F., Zheng, Q.-S.: An analytical model of effective electrical conductivity of carbon nanotube composites. *Appl. Phys. Lett.* **92**, 071902 (2008)
- Duan, H.L., Karihaloo, B.L.: Effective thermal conductivities of heterogeneous media containing multiple imperfectly bonded inclusions. *Phys. Rev. B.* **75**, 064206 (2007)
- Duan, H.L., Karihaloo, B.L., Wang, J., Yi, X.: Effective conductivities of heterogeneous media containing multiple inclusions with various spatial distributions. *Phys. Rev. B.* **73**, 174203 (2006)
- Dunn, M.L., Taya, M.: The effective thermal conductivity of composites with coated reinforcement and the application to imperfect interfaces. *J. Appl. Phys.* **73**, 1711–1722 (1993)
- Eshelby, J.D.: The determination of the elastic field of an ellipsoidal inclusion, and related problems. *Proc. R. Soc. London A.* **241**, 376–396 (1957)
- Feng, C., Jiang, L.: Micromechanics modeling of the electrical conductivity of carbon nanotube (CNT)–polymer nanocomposites. *Compos. Part A Appl. Sci. Manuf.* **47**, 143–149 (2013)
- Gao, L., Li, Z.: Effective medium approximation for two-component nonlinear composites with shape distribution. *J. Phys. Condens. Matter.* **15**, 4397 (2003)
- Gardea, F., Lagoudas, D.C.: Characterization of electrical and thermal properties of carbon nanotube/epoxy composites. *Compos. Part B Eng.* **56**, 611–620 (2014)
- Geim, A.K., Novoselov, K.S.: The rise of graphene. *Nat. Mater.* **6**, 183–191 (2007)
- Hashin, Z.: Thin interphase/imperfect interface in conduction. *J. Appl. Phys.* **89**, 2261–2267 (2001)
- Hashin, Z., Shtrikman, S.: A variational approach to the theory of the effective magnetic permeability of multiphase materials. *J. Appl. Phys.* **33**, 3125–3131 (1962)
- Hatta, H., Taya, M.: Effective thermal conductivity of a misoriented short fiber composite. *J. Appl. Phys.* **58**, 2478–2486 (1985)
- He, L., Tjong, S.C.: Low percolation threshold of graphene/polymer composites prepared by solvothermal reduction of graphene oxide in the polymer solution. *Nanoscale Res. Lett.* **8**, 1–7 (2013)
- Hernández, J.J., García-Gutiérrez, M.C., Nogales, A., Rueda, D.R., Kwiatkowska, M., Szymczyk, A., Roslaniec, Z., Concheso, A., Guinea, I., Ezquerro, T.A.: Influence of preparation procedure on the conductivity and transparency of SWCNT-polymer nanocomposites. *Compos. Sci. Technol.* **69**, 1867–1872 (2009)
- Hill, R.: A self-consistent mechanics of composite materials. *J. Mech. Phys. Solids.* **13**, 213–222 (1965)
- Landauer, R.: The electrical resistance of binary metallic mixtures. *J. Appl. Phys.* **23**, 779–784 (1952)
- Li, C., Chou, T.-W.: Continuum percolation of nanocomposites with fillers of arbitrary shapes. *Appl. Phys. Lett.* **90**, 174108 (2007)
- Li, J., Ma, P.C., Chow, W.S., To, C. K., Tang, B.Z., Kim, J.K.: Correlations between percolation threshold, dispersion state, and aspect ratio of carbon nanotubes. *Adv. Funct. Mater.* **17**, 3207–3215 (2007b)
- Li, C., Thostenson, E.T., Chou, T.-W.: Dominant role of tunneling resistance in the electrical conductivity of carbon nanotube–based composites. *Appl. Phys. Lett.* **91**, 223114 (2007a)

- Ma, H.M., Gao, X.-L., Tolle, T.B.: Monte Carlo modeling of the fiber curliness effect on percolation of conductive composites. *Appl. Phys. Lett.* **96**, 061910 (2010)
- Martin, C.A., Sandler, J.K.W., Shaffer, M.S.P., Schwarz, M.K., Bauhofer, W., Schulte, K., Windle, A.H.: Formation of percolating networks in multi-wall carbon-nanotube-epoxy composites. *Compos. Sci. Technol.* **64**, 2309–2316 (2004)
- Maxwell, J. C. *A Treatise on Electricity and Magnetism*, Vol. 1, 3rd ed. (Clarendon Press, Oxford, original 1891, reproduced 1982), p. 435–441
- McLachlan, D.S., Chiteme, C., Park, C., Wise, K.E., Lowther, S.E., Lillehei, P.T., Siochi, E.J., Harrison, J.S.: AC and DC percolative conductivity of single wall carbon nanotube polymer composites. *J. Polym. Sci. Part B Polym. Phys.* **43**, 3273–3287 (2005)
- Mori, T., Tanaka, K.: Average stress in matrix and average elastic energy of materials with misfitting inclusions. *Acta Metall.* **21**, 571–574 (1973)
- Nan, C.-W., Birringer, R., Clarke, D.R., Gleiter, H.: Effective thermal conductivity of particulate composites with interfacial thermal resistance. *J. Appl. Phys.* **81**, 6692–6699 (1997)
- Nan, C.-W., Shen, Y., Ma, J.: Physical properties of composites near percolation. *Annu. Rev. Mater. Res.* **40**, 131–151 (2010)
- Ngabonziza, Y., Li, J., Barry, C.F.: Electrical conductivity and mechanical properties of multi-walled carbon nanotube-reinforced polypropylene nanocomposites. *Acta Mech.* **220**, 289–298 (2011)
- Pan, Y., Weng, G.J., Meguid, S.A., Bao, W.S., Zhu, Z.-H., Hamouda, A.M.S.: Percolation threshold and electrical conductivity of a two-phase composite containing randomly oriented ellipsoidal inclusions. *J. Appl. Phys.* **110**, 123715 (2011)
- Pang, H., Chen, T., Zhang, G., Zeng, B., Li, Z.-M.: An electrically conducting polymer/graphene composite with a very low percolation threshold. *Mater. Lett.* **64**, 2226–2229 (2010)
- Prasher, R., Evans, W., Meakin, P., Fish, J., Phelan, P., Koblinski, P.: Effect of aggregation on thermal conduction in colloidal nanofluids. *Appl. Phys. Lett.* **89**, 143119 (2006)
- Reinecke, B.N., Shan, J.W., Suabedissen, K.K., Cherkasova, A.S.: On the anisotropic thermal conductivity of magnetorheological suspensions. *J. Appl. Phys.* **104**, 023507 (2008)
- Seidel, G.D., Lagoudas, D.C.: A micromechanics model for the electrical conductivity of nanotube-polymer nanocomposites. *J. Compos. Mater.* **43**, 917–941 (2009)
- Srivastava, N.K., Mehra, R.M.: Study of structural, electrical, and dielectric properties of polystyrene/foiated graphite nanocomposite developed via in situ polymerization. *J. Appl. Polym. Sci.* **109**, 3991–3999 (2008)
- Stankovich, S., Dikin, D.A., Dommett, G.H.B., Kohlhaas, K.M., Zimney, E.J., Stach, E.A., Piner, R.D., Nguyen, S.T., Ruoff, R.S.: Graphene-based composite materials. *Nature*. **442**, 282–286 (2006)
- Tkalya, E., Ghislandi, M., Otten, R., Lotya, M., Alekseev, A., van der Schoot, P., Coleman, J., de With, G., Koning, C.: Experimental and theoretical study of the influence of the state of dispersion of graphene on the percolation threshold of conductive graphene/polystyrene nanocomposites. *ACS Appl. Mater. Interfaces*. **6**, 15113–15121 (2014)
- Wang, Y., Weng, G.J., Meguid, S.A., Hamouda, A.M.: A continuum model with a percolation threshold and tunneling-assisted interfacial conductivity for carbon nanotube-based nanocomposites. *J. Appl. Phys.* **115**, 193706 (2014)
- Wang, Y., Shan, J.W., Weng, G.J.: Percolation threshold and electrical conductivity of graphene-based nanocomposites with filler agglomeration and interfacial tunneling. *J. Appl. Phys.* **118**, 065101 (2015)
- Weng, G.J.: Some elastic properties of reinforced solids, with special reference to isotropic ones containing spherical inclusions. *Int. J. Eng. Sci.* **22**, 845–856 (1984)
- Weng, G.J.: The theoretical connection between Mori-Tanaka's theory and the Hashin-Shtrikman-Walpole bounds. *Int. J. Eng. Sci.* **28**, 1111–1120 (1990)
- Weng, G.J.: A dynamical theory for the Mori-Tanaka and Ponte Castañeda-Willis estimates. *Mech. Mater.* **42**, 886–893 (2010)
- Xie, S.H., Liu, Y.Y., Li, J.Y.: Comparison of the effective conductivity between composites reinforced by graphene nanosheets and carbon nanotubes. *Appl. Phys. Lett.* **92**, 243121 (2008)